Geochimica et Cosmochimica Acta 388 (2025) 48–60

Contents lists available at ScienceDirect

Geochimica et Cosmochimica Acta

journal homepage: www.elsevier.com/locate/gca

Multi-isotopic (Fe-Cu-Zn) constraints on the magmato-hydrothermal history during mantle exhumation at slow-spreading centers

R. Coltat [a,*], B. Debret [b], R. Tilhac [a], M. Andreani [c,d], C.G.C. Patten [e], M. Godard [f], J. Escartín [g]

[a] Instituto Andaluz de Ciencias de la Tierra (IACT), CSIC, Armilla, Granada, Spain
[b] Université Paris Cité, Institut de physique du globe de Paris, CNRS, Paris, France
[c] Laboratoire de Géologie de Lyon, UMR 5672, ENS, Université Lyon 1, Lyon, France
[d] Institut Universitaire de France, France
[e] Institute of Mineralogy and Petrography, University of Innsbruck, Innsbruck, Austria
[f] Géosciences Montpellier, CNRS, Université de Montpellier, Montpellier, France
[g] Laboratoire de Géologie, UMR 8538, Département de Géosciences, Ecole Normale Supérieure de Paris, PSL Research University, Paris, France

ARTICLE INFO

Associate Editor: Batrice Luais

Keywords:
Non-traditional stable isotopes
Oceanic lithospheric mantle
Transition metals
Hydrothermal alteration
Kinetic isotope fractionation
Mid-Atlantic Ridge Kane area

ABSTRACT

At slow to ultraslow-spreading ridges, tectonic mantle exhumation and magmatic processes accounts for heterogeneity in the lithosphere and drives deep hydrothermal circulation and fluids venting at the seafloor. However, the spatio-temporal evolution and the interplay between magmatic and hydrothermal processes during mantle exhumation, as well as their consequences for chemical exchange at mid-ocean ridges are poorly constrained.

We carried out a Fe, Cu and Zn isotope study of mantle rocks drilled at the Mid-Atlantic Ridge Kane (MARK) area (23′30°N) to decipher the consequences of magmatic versus hydrothermal chemical exchange on lithospheric mantle composition. At MARK, mantle rocks undergo complex melt-rock interaction during melt percolation overprinted by high temperature (HT, > 350 °C) hydrothermal circulation that leads to the formation of secondary mineral assemblages (e.g., amphibole, chlorite, ilvaite, hydro-andradite, clinopyroxene, talc, serpentine). Serpentinized peridotites cut by hydrothermally overprinted magmatic veins have increased isotopic heterogeneity to both lighter and heavier isotope compositions (δ^{56}Fe from −0.44 to 0.07 ± 0.03 ‰; δ^{66}Zn from −0.24 to 0.32 ± 0.04 ‰), expending the predictive unaltered composition of the primitive mantle (δ^{56}Fe = 0.025 ± 0.025 ‰ and δ^{66}Zn = 0.16 ± 0.06 ‰). Such variability is ascribed to diffusion-related kinetic isotope fractionation during the percolation of Fe- and Zn-rich melt in mantle rocks. Low isotopic values are due to preferential diffusion of lighter isotope in mantle rocks, while high values may involve mixing of serpentinized peridotites with isotopically heavy magmatic veins. The lower Cu content (0.5 to 23.9 ppm) and either lower or higher δ^{65}Cu (−0.11 to 0.32 ± 0.04 ‰) of abyssal peridotites, compared to the primitive mantle (30 ppm Cu, δ^{65}Cu = 0.07 ± 0.1 ‰), can be explained through Cu leaching during hydrothermal alteration of sulfide, and possibly oxide, at high temperature (~ 450–600 °C). Hydrothermal veins in serpentinites formed at decreasing temperature (~ 300 °C) from a metal- and sulfur-rich fluid interacting with serpentinized peridotites. Iron, Cu and Zn isotopes record the inventory of magmato-hydrothermal processes during mantle exhumation at (ultra-) slow spreading centers, from HT melt-rock interaction to late low-temperature (LT) fluid-rock interaction.

1. Introduction

Mid-Ocean Ridges (MORs) are the locus of thermo-chemical exchanges between the lithosphere and oceans, accounting for mass transfer and contributing to lithosphere cooling (Humphris and Klein, 2018). At slow to ultraslow-spreading ridges, mantle exhumation commonly accommodates lithospheric divergence (e.g., Escartín and Olive, 2022). Hydrothermal fluid circulation in the lithospheric mantle may allow seafloor massive sulfide deposits (e.g., Fouquet et al., 2010; Debret et al., 2018) and LT carbonate-brucite chimneys to form (e.g., Lost City hydrothermal field; Kelley et al., 2001). These chemical exchanges between the fluid and mantle rocks have not only strong

* Corresponding author.
E-mail address: remi.coltat@univ-orleans.fr (R. Coltat).

https://doi.org/10.1016/j.gca.2024.11.013
Received 6 February 2024; Accepted 13 November 2024
Available online 19 November 2024

implications on metal and volatile cycling in the lithospheric mantle but also on deep-life development (Van Dover, 2019) as well as chemical and redox exchanges in subduction zones (e.g., Debret and Sverjensky, 2017). Unravelling the nature of fluids venting at the seafloor requires a thorough evaluation of the deep melt-rock and fluid-rock interactions. However, this is hampered by i) limited exposure at the seafloor and difficulty sampling *in situ* (e.g., ROV or submersible dives) and ii) extensive seafloor weathering of exposed rocks. An alternative is to turn to drill cores, although they are scarce from mantle-dominated MOR environments and generally only penetrate the shallow subseafloor.

Non-traditional stable isotopes, for example Fe, Cu or Zn, have been recently used to provide valuable constraints on magmatic and hydrothermal processes in the oceanic lithosphere (e.g., Debret et al., 2018; Liu et al., 2019; Wang et al., 2023). Mantle partial melting produces minor and predictable fractionation of Fe, Cu and Zn isotopes (< 0.1 ‰), in all cases leaving a melt slightly enriched in the heavier isotopes (Weyer and Ionov, 2007; Ikehata and Irata, 2012; William and Bizimis, 2014; Liu et al., 2015a,b; Wang et al., 2017; Sossi et al., 2018). In contrast, post-melting, HT melt-rock interaction to LT hydrothermalism may significantly affect the transition metal isotopic compositions of peridotites. For instance, element diffusion induced during melt or fluid metasomatism may drastically modify the Fe (up to ~ 0.5 %; Weyer and Ionov, 2007; Zhao et al., 2015) and Zn isotope compositions (up to ~ 0.5 %; Wang et al., 2017; Fang et al., 2022) of metasomatized peridotites, while sulfide breakdown or formation may significantly fractionate Cu isotopes (up to ~ 2 ‰; Liu et al., 2015a,b). Theory predicts that LT hydrothermal processes can induce larger stable isotope fractionations than HT processes. However, limited isotope fractionation was reported during LT peridotite serpentinization in seawater-dominated systems at the seafloor (Pons et al., 2011; Craddock et al., 2013; Scott et al., 2017). In contrast, HT (> 350 °C) deep fluid circulations appear to lead to contrasting Fe, Zn or Cu isotopic signatures in abyssal serpentinites (Debret et al., 2018). These are particularly sensitive to the temperature of formation (Fujii et al., 2013), nature of ligands complexing metals (e.g., Fujii et al., 2014; Moynier et al., 2017) and metal sources (i.e., silicates, oxides, sulfides; Liu et al., 2021). Transition metal isotopes may then help unravelling different magmatic and hydrothermal processes during mantle exhumation at slow- to ultraslow-spreading centers. However, the study of non-traditional stable isotopes in hydrothermal systems at mid-ocean ridges is still largely restricted to seafloor massive sulfide deposits and hydrothermal fluids (e.g., Beard et al., 2003; Rouxel et al., 2004; John et al., 2008; Wang et al., 2023) or dredged weathered peridotites (Liu et al., 2019), whilst studies of these non-traditional stable isotopes in deep-seated HT magmatic and hydrothermal processes in abyssal mantle rocks remain scarce.

In this study, we focus on the Mid-Atlantic Ridge Kane (MARK) area where exhumed serpentinized peridotites and magmatic intrusions were drilled during ODP Leg 153 (Cannat et al., 1995). A degree of serpentinization as low as < 20 % is recorded by serpentinized peridotites at the contact with magmatic intrusions (Andreani et al., 2007), preserving mineralogical assemblages formed at HT (> 350 °C) and offering the opportunity to study the magmato-hydrothermal processes that occur prior to or during early serpentinization (Coltat et al., 2023). These include early melt-peridotite interaction, subsequent hydrothermal alteration of magmatic veins (i.e., pyroxenite and gabbroic veins) and transformation of magmatic silicates to secondary amphibole, clinopyroxene, chlorite, talc, garnet, serpentine, and late hydrothermal veining in serpentinites forming Fe-Ca silicates and sulfides (Coltat et al., 2023). We performed Fe, Cu, Zn isotope analyses in abyssal peridotites to i) decipher the behavior of metals during melt-rock and fluid-rock interactions and ii) unravel the physico-chemical conditions of fluid-rock interaction, aiming at providing constraints on metal mobility at MORs.

2. Geological setting of the Mid-Atlantic Ridge Kane area (23°30′ N MAR) and sampling

2.1. Geological setting

The southern intersection between the Kane fracture zone and the axial rift valley is referred to as the MARK area, 23°30′N (Fig. 1A, B). The western wall of the MARK area is an inside corner, forming a dome-like topographic high (Fig. 1B, Cannat et al., 1995), namely the Kane megamullion (Dick et al., 2008). The presence of serpentinites cropping out along a 2 km-wide belt that extends at least 20 km parallel to the MAR axis in the western wall of the MAR axial valley was confirmed by submersible dives (Karson et al., 1987). The conjugate crust (i.e., east of the MAR) exhibits a deeper bathymetry (> 3500 m), less steep topography and exposes block-faulted basaltic pillow lavas (Cannat et al., 1995). The axial valley hosts the median neovolcanic ridge that extends 40 km south to the Kane transform fault (Fig. 1B; Cannat et al., 1995), hosting the active Snake Pit hydrothermal field. The full spreading rate here is ~ 2.5 cm/year (Schulz et al., 1988).

ODP Site 920 is located at 23°20.32′N, 40-km south of the Kane transform fault at a depth of ~ 3300 m below sea level (Fig. 1, Cannat et al., 1995). During ODP Leg 153, serpentinized harzburgites with minor gabbroic veins were drilled at Holes 920B and 920D, reaching depths of 126 and 200 m below the seafloor, cumulative recovery rates of 38 % and 47 %, respectively (Fig. 1C; Cannat et al., 1995). Despite pervasive serpentinization of the MARK mantle rocks, primary textures are well-preserved. Serpentine-rich shear zones mimic the shallow E-dipping fabrics of mantle rocks. These structures are almost parallel to a HT crystal-plastic fabric carried by oriented olivine and elongated pyroxene grains (Mével et al., 1991). This supports a model in which fluid circulation and serpentinization occurred during mantle exhumation at MARK (Andreani et al., 2007).

Oxygen and sulfur isotope compositions of the MARK serpentinites suggest serpentinization temperatures from > 350–400 °C down to 200 °C (Agrinier and Cannat, 1997; Alt and Shanks, 2003), typical of (sub) greenschist metamorphic conditions. However, mineralogical assemblages and sulfur element and isotope compositions of serpentinites point to a high temperature hydrothermal event prior to serpentinization (Cannat et al., 1995; Alt and Shanks, 2003), suggesting changes in hydrothermal regimes over time. Mafic rocks intruding serpentinites recorded similar variable hydrothermal conditions from amphibolite to greenschist metamorphic conditions, while local rodingitization of mafic rocks suggests interaction with a serpentinization-derived fluid (Cannat et al., 1995). A Fe-Ca-metasomatism forming ilvaite, hydrogarnet, diopside, amphibole and carbonate occurs in mantle rocks locally close to magmatic veins (Gaggero et al., 1997; Coltat et al., 2023). Coltat et al. (2023) propose a two-step process to explain Fe-Ca metasomatism. First, melt percolation in peridotites promotes melt-rock interaction and Fe, Co, Zn supply in the surrounding mantle silicates. Subsequent HT (> 350 °C) fluid circulation and alteration of magmatic intrusions mobilizes Ca and Cu, forming the above mineral assemblages. Late fluid circulation during serpentinization (< 400 °C) produces hydrothermal veins and associated oxide (magnetite) and sulfide (pyrrhotite and chalcopyrite). Metals might derive from the leaching of primary mantle and magmatic sulfides during intense serpentinization and alteration of magmatic rocks, respectively (Gaggero et al., 1997; Coltat et al., 2023).

2.2. Sampling strategy

We focused our study on 15 mantle rock samples described by Coltat et al. (2023), forming 3 distinct petrographic and geochemical groups. The first group consists of serpentinized peridotites. The second and third groups are serpentinized peridotites either cut by hydrothermally overprinted magmatic veins or hydrothermal veins, respectively. This sample suite records the magmato-hydrothermal history during mantle

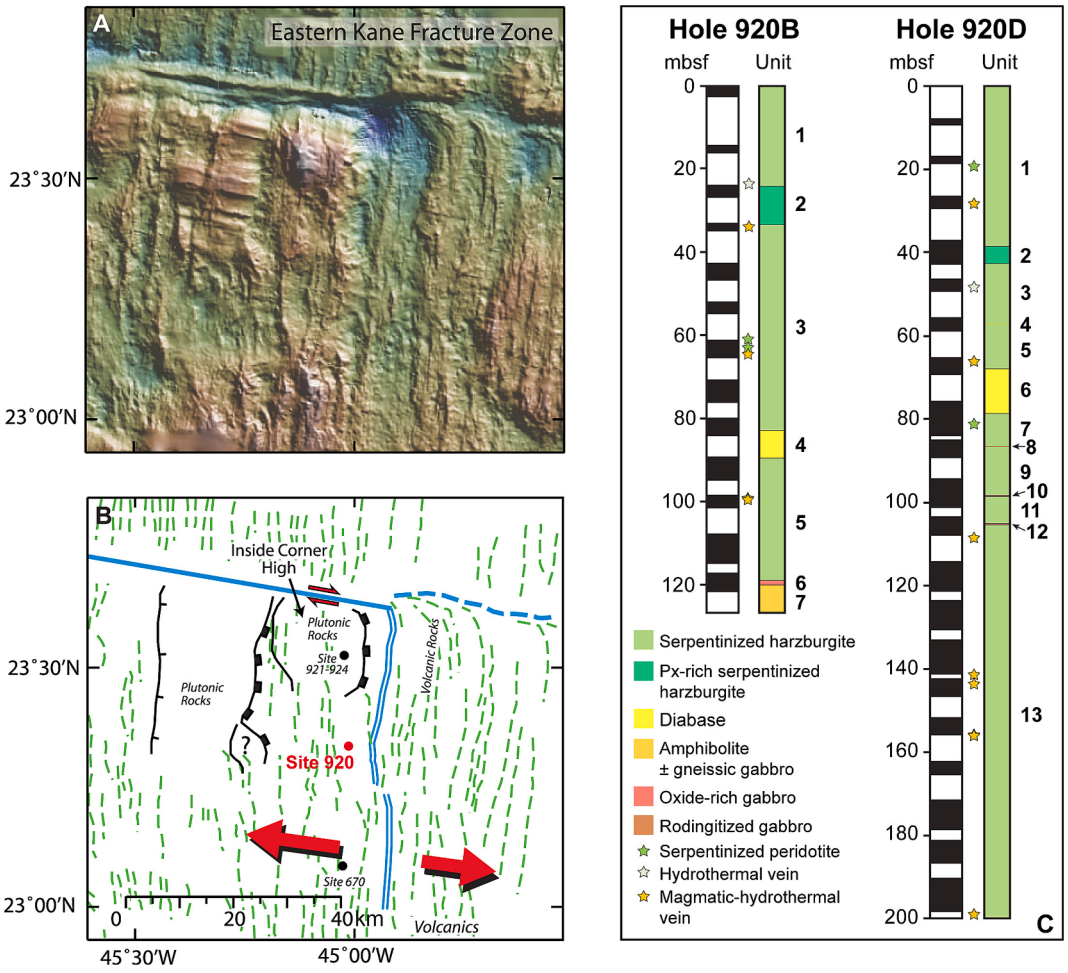

Fig. 1. (A) Shaded relief bathymetric map of the Mid-Atlantic Ridge Kane area. (B) Tectonic interpretation of the MARK area (modified after Dick et al., 2008). Green dashed lines are ridge-parallel volcanic lineaments, heavy tabbed lines are detachment fault zone terminations, light tabbed lines are detachment breakaway zones. Active transform fault zone displayed as continuous blue line and its inactive trace by dashed blue line. Double blue line shows the ridge axis. ODP sites displayed as full circles. (C) Lithological logs of the Holes 920B and 920D showing the sample location (modified after Cannat et al., 1995).

exhumation with i) melt percolation and melt-rock interaction in the peridotite basement, ii) HT hydrothermal alteration responsible for the formation of (Fe-)Ca mineral phases, and iii) serpentinization and late hydrothermal veining at lower temperatures. Geochemical compositions of the MARK mantle rocks are given in Table 1 and are published in Coltat et al. (2023). Samples from the second and third groups represent mechanical mixing between veins and the serpentinized peridotites.

MARK serpentinized peridotites (SPs) analyzed in this study have Al_2O_3/SiO_2 ranging between 0.02 and 0.03, typical of harzburgite, and higher than typical refractory peridotites (Godard et al., 2008). They have slightly lower MgO content (44.39–49.84 wt% on a volatile-free basis) and Mg# (90 to 92) than MARK SPs reported in the literature (Fig. 2A). One dunite and one plagioclase-impregnated SP have high FeO (8.08–8.82 wt% on a volatile-free basis), Nb (0.038 and 0.039 ppm) contents and high chondrite-normalized Gd_N/Lu_N (0.47 and 0.75), compared to common MARK SPs, pointing to melt-rock interaction in those samples (Paulick et al., 2006). This is due to the high solubility of high strength field element (HFSE, e.g., Nb) in silicic melts (Paulick et al., 2006). Overall, the two other SPs, although having low MgO content, are indistinguishable from the MARK SPs reported in the literature.Serpentinized peridotites cut by hydrothermally overprinted magmatic veins (MPs) have high Al_2O_3/SiO_2 (0.02–0.2), Gd_N/Lu_N (0.52–1.15), FeO (8.04–11.68 wt% on a volatile-free basis) and Nb contents (0.027–2.195 ppm), and low Mg# (81–90, Fig. 2), in good agreement with the magmatic (i.e., pyroxenite/mafic) origin of the veins (Coltat et al., 2023). Most of these have higher FeO content than the MARK serpentinized peridotites (average at about 7.25 wt% FeO), the primitive mantle (8.08 wt% FeO, McDonough and Sun, 1995) and the depleted MORB mantle (8.18 wt% FeO, Workman and Hart, 2005). Hence, we interpret MPs as products of melt-rock interaction overprinted by HT fluid-rock interaction forming secondary mineral assemblages.

Serpentinized peridotites cut by hydrothermal veins (HPs) have low Al_2O_3/SiO_2 (0.02–0.04), MgO (33.82–43.32 wt% on a volatile-free basis), FeO (6.41–7.12 wt% on a volatile-free basis) and Nb contents (0.004–0.009 ppm), while they present high Rb/Nb (54–62.2; Fig. 2). The high Rb/Nb is a combination of low Nb contents (Fig. 2B) and Rb addition to the rock during vein formation (Fig. 2C), according to the high solubility of large ion lithophile elements (LILE, e.g., Rb) in hydrothermal fluids (Palmer and Edmond, 1989), while HFSE are poorly soluble (Paulick et al., 2006).

3. Methods

About 50 mg of powdered samples were dissolved using a 1:1 mix of concentrated HF and HCl in square bodied Teflon vials (© Savillex) at 150 °C in an oven for 5 days. These were then further digested with aqua regia, a 1:3 mix of concentrated HNO_3 and HCl for 3 days at 130 °C. Finally, samples were brought into solution in 6 M HCl prior to column chemistry. The whole procedure ensures full dissolution of refractory

Table 1
Compositions for selected geochemical markers and Fe, Cu and Zn isotope compositions of mantle rocks of the MARK area (ODP Leg 153).

Sample	Type	Vein mineralogy	Vein vol.	δ^{56}Fe		δ^{57}Fe			δ^{65}Cu			δ^{66}Zn		δ^{68}Zn			FeO^{a}_{tot}	MgO^{a}	Al_2O_3/SiO_2	Cu	Zn	Rb	Nb	Gd_N/Lu_N	Rb/Nb
			(%)	‰	2sd	‰	2sd	*n*	‰	2sd	*n*	‰	2sd	‰	2sd	*n*	wt. %	wt. %		ppm	ppm	ppm	ppm		
920B-3R-1, 2–5	HP	Srp, Cal, Ccp	100	−0.13	0.02	−0.19	0.04	3	0.02	0.02	5	0.27	0.05	0.57	0.10	4	6.41	43.32	0.04	119.6	126	0.487	0.009	0.09	53.98
920D-6R-2, 28–31	HP	Cpx, Srp, Grt, Cal, Po	40	−0.30	0.04	−0.48	0.09	2	−0.19	0.02	5	0.34	0.06	0.67	0.09	4	7.12	33.82	0.02	247.5	317	0.225	0.004	0.22	62.19
920D-3R-2, 4–7	SP	Srp	N.A.	−0.23	0.03	−0.33	0.09	4	0.25	0.07	5	0.35	0.04	0.72	0.09	3	8.08	44.84	0.02	41.1	37	0.220	0.039	0.47	5.57
920B-7R-1, 21–22	SP	Srp	N.A.	−0.12	0.03	−0.23	0.05	3	0.00	0.05	5	0.18	0.03	0.37	0.07	5	7.56	40.39	0.03	42.4	88	0.399	0.009	0.19	46.08
920B-7R-2, 67–68	SP	Srp	N.A.	−0.19	0.01	−0.31	0.06	3	0.18	0.06	5	0.09	0.06	0.23	0.14	4	6.77	41.28	0.02	117.9	53	0.189	0.009	0.19	20.55
920D-10R-3, 0–4	SP	Srp	N.A.	−0.39	0.05	−0.55	0.08	3	0.16	0.02	4	0.05	0.02	0.14	0.03	5	8.82	43.90	0.03	4.0	58	0.069	0.038	0.75	1.81
920B-4R-1, 76–77	MP	Srp, Amp, Chl, Tlc	30	−0.20	0.01	−0.28	0.02	3	−0.10	0.06	5	0.24	0.06	0.55	0.12	5	8.37	38.34	0.08	17.5	60	0.372	0.650	0.99	0.57
920B-7R-3, 82–84	MP	Srp, Amp, Chl	30	−0.44	0.02	−0.66	0.06	3	0.32	0.04	3	0.07	0.04	0.13	0.06	5	9.30	44.62	0.03	1.0	46	0.046	0.027	0.55	1.68
920D-4R-1, 80–81	MP	Cpx, Srp, Chl, Amp, Cal, Mag	90	0.07	0.02	0.08	0.04	2	−0.11	0.03	5	0.16	0.05	0.37	0.10	5	8.04	28.56	0.06	18.8	41	0.170	1.113	1.15	0.15
920D-8R-1, 12–13	MP	Chl, Cal, Srp, Sulf	10	0.00	0.02	−0.03	0.00	2	0.06	0.04	5	0.15	0.07	0.31	0.10	5	8.46	40.81	0.05	23.9	59	0.175	0.230	0.72	0.76
920D-13R-4, 5–9	MP	Srp, Chl	5	−0.02	0.03	−0.02	0.07	4	0.15	0.05	2	0.08	0.03	0.23	0.05	3	9.24	43.38	0.03	5.6	44	0.093	0.079	0.51	1.17
920D-16R-7, 19–22	MP	Srp, Chl, Amp, Cpx, Tlc	25	−0.25	0.06	−0.34	0.10	3	−0.07	0.03	2	0.32	0.05	0.64	0.06	4	11.68	42.11	0.02	1.9	39	0.059	0.219	0.63	0.27
920D-17R-1, 46–48	MP	Srp, Amp, Chl, Tlc, Ttn	50	−0.06	0.02	−0.08	0.02	4				−0.24	0.06	−0.44	0.12	5	9.67	22.49	0.20	0.5	41	0.112	2.195	1.01	0.05
920D-18R-3, 29–33	MP	Amp, Srp, Cpx	35	−0.18	0.03	−0.28	0.10	3	0.38	0.05	5	0.15	0.01	0.37	0.04	2	10.27	37.95	0.03	3.5	36	0.109	0.305	1.11	0.36
920D-18R-3, 48–54	MP	Cpx, Srp	10	−0.37	0.04	−0.59	0.10	3	0.24	0.01	5	0.10	0.04	0.20	0.07	5	11.19	41.91	0.03	23.9	50	0.033	0.055	0.55	0.60
UB-N	RM			0.02	0.04	0.02	0.10	5	0.06	0.03	6	0.32	0.06	0.66	0.10	4									
preferred values	RM			0.06	0.03	0.08	0.05		0.06			0.38	0.09	0.73	0.30										
JP1	RM			0.00	0.05	0.00	0.05	4	0.06	0.05	4	0.13	0.01	0.31	0.02	2									
preferred values	RM			0.00	0.05			3	0.03	0.05	3	0.22	0.04	0.43	0.06	6									

"Vein vol." denotes the volume of magmatic hydrothermally overprinted and hydrothermal veins (serpentine veins are not considered) mixed with the host serpentinite (from Coltat et al., 2023).
[a]geochemical compositions given on a volatile-free basis. HP = serpentinized peridotite cut by hydrothermal vein; SP = serpentinized peridotite; MP = serpentinized peridotite cut by hydrothermally overprinted magmatic vein; RM = reference material.
Srp = serpentine, Tlc = talc, Chl = chlorite, Amp = amphibole, Cpx = clinopyroxene, Grt = hydro-garnet, Ttn = titanite, Cal = calcite, Mag = magnetite, Sulf = sulfides, Ccp = chalcopyrite, Po = pyrrhotite.
Preferred values for UB-N are from Bishop et al. (2012) for Cu and Telus et al. (2012) for Fe and Zn, preferred values for JP1 are from Weyer et al. (2005) for Fe, Liu et al. (2015a,b) for Cu, Wang et al. (2017) for Zn.

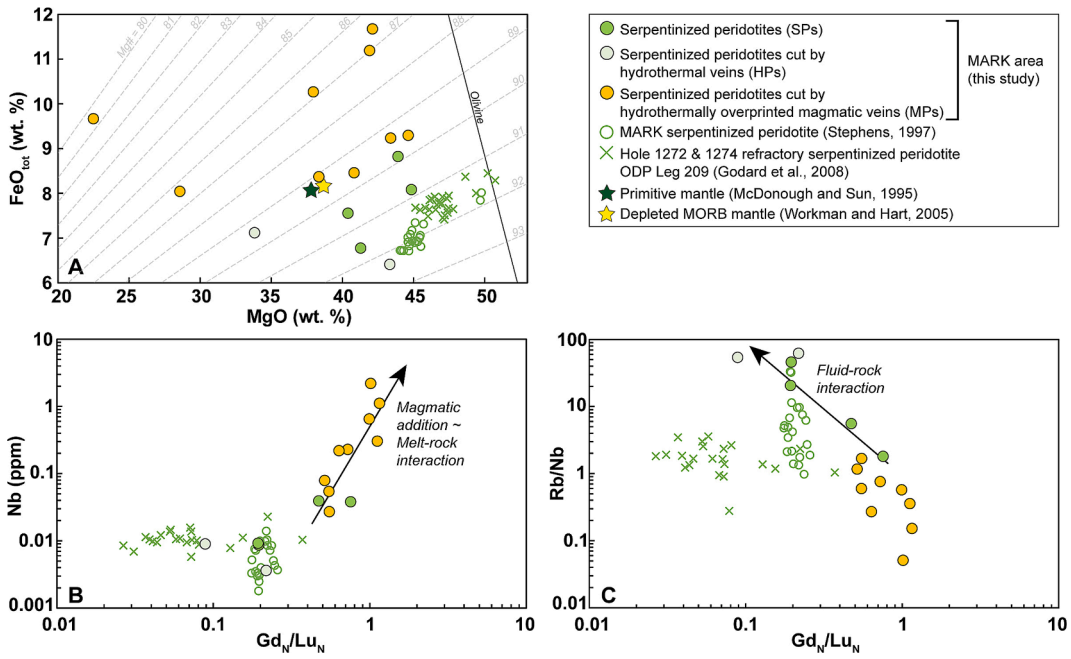

Fig. 2. Selected geochemical markers of MARK mantle rocks (from Coltat et al., 2023) plotted against data from the literature. Serpentinized peridotites of ODP Leg 209 are plotted for comparison with highly depleted mantle rocks. (A) FeO_{tot} vs. MgO (wt. %, volatile-free basis). Dotted lines are *iso*-Mg#. (B) Nb (ppm) and (C) Rb/Nb vs. chondrite-normalized Gd/Lu (CI compositions from McDonough and Sun, 1995).

phases such as spinels (see Debret et al., 2021). Quantitative purification of Zn, Cu and Fe was achieved by chromatographic exchange, using 1 ml of AG1-x8 (200–400 mesh) and 0.4 × 7 cm Teflon columns, following the procedure of Sossi et al. (2015). The total procedural blank contribution was < 80 ng for Fe, < 15 ng for Zn and < 1 ng for Cu which is negligible with respect to the total amount of dissolved sample (blank contribution ≪ 1 %).

3.1. Fe isotope analyses

Bulk-rock Fe isotope data were obtained at Institut de Physique du Globe de Paris (IPGP) on a Neptune Plus MC-ICP-MS in wet plasma and high-resolution mode. Instrumental mass bias was corrected by sample standard bracketing. Both sample and standard solutions were run at 2 ppm in 0.5 M HNO_3, giving the same total beam intensity of 14 V using a 10^{11} Ω resistor. Isotope ratios are reported as per-mil notation relative to the IRMM-014 external standard (δ^{56}Fe), and δ^{57}Fe is given to demonstrate mass dependency of the measurements. All reported errors are 2 standard deviations (2sd, n = 2–5).

$$\delta^{56}Fe = \left(\left({}^{56}Fe/{}^{54}Fe_{sample}\right)/\left({}^{56}Fe/{}^{54}Fe_{IRMM-014}\right) - 1\right) \times 10^3$$
$$\delta^{57}Fe = \left(\left({}^{57}Fe/{}^{54}Fe_{sample}\right)/\left({}^{57}Fe/{}^{54}Fe_{IRMM-014}\right) - 1\right) \times 10^3$$

In addition to Fe masses, ^{53}Cr and ^{60}Ni were also monitored and online Cr and Ni corrections were applied to account for any isobaric interference of ^{54}Cr and ^{58}Ni on the ^{54}Fe and ^{58}Fe, respectively. These corrections were either negligible or non-existent demonstrating the effective separation of Fe from Cr and Ni during column chemistry. A FeCl standard solution was analyzed throughout each analytical session giving an average δ^{56}Fe value of −0.76 (±0.05) ‰ and average δ^{57}Fe value of −1.13 (±0.09) ‰ (2sd, n = 20), in excellent agreement with previous studies (e.g., Williams and Bizimis, 2014). In addition, reference materials (JP-1 peridotite and UB-N serpentinite) were processed through columns and analyzed as unknown. They gave accurate δ^{56}Fe values of 0.00 ± 0.05 ‰ and 0.02 ± 0.04 ‰ and δ^{57}Fe values of 0.00 ± 0.05 ‰ and 0.02 ± 0.1 ‰ for JP-1 (n = 4) and UB-N (n = 5), respectively, in agreement with previous studies (Weyer et al., 2005; Telus et al., 2012) (Table 1).

3.2. Cu and Zn isotope analyses

Bulk-rock Cu and Zn isotope data were obtained at IPGP on a Neptune Plus MC-ICP-MS in wet plasma and low-resolution mode. Each sample was bracketed by standard analyses (either Zn AA-ETH standard or an IPGP Cu in-house). Both sample and standard solutions were run at 100 ppb in 0.5 M HNO_3, giving the same total beam intensity of 6 V using a 10^{11} Ω resistor. In addition to Cu and Zn masses, we also monitored ^{62}Ni to check for interference of ^{64}Ni on ^{64}Zn. However, the ^{62}Ni signal was systematically lower than the background, which indicates effective Ni separation.

Copper isotope ratios are reported as a delta value in permil notation relative to the NIST SRM 976 Cu isotopic standard (δ^{65}Cu). All reported errors are 2 standard deviations (2sd, n = 2–5):

$$\delta^{65}Cu = (({}^{65}Cu/{}^{63}Cu_{sample}) / ({}^{65}Cu/{}^{63}Cu_{NIST976}) - 1) \times 10^3.$$

Samples were measured relative to an in-house IPGP standard offset from NIST SRM 976 Cu by 0.31 ± 0.03 ‰ (long term reproducibility, see for example Guinoiseau et al., 2017). During data acquisition, ERM-AE647 was analyzed as unknown throughout the Cu session, giving a mean δ^{65}Cu value of 0.17 ± 0.05 ‰ (n = 19), in excellent agreement with previous studies (Moeller et al., 2012).

Zinc isotope ratios are reported as a delta value in permil notation relative to the JMC-Lyon isotopic standard (δ^{66}Zn). δ^{68}Zn are also given to demonstrate mass dependency of the measurements. All reported errors are 2 standard deviations (2sd, n = 2–5).

$$\delta^{66}Zn = \left(\left({}^{66}Zn/{}^{64}Zn_{sample}\right)/\left({}^{66}Zn/{}^{64}Zn_{JMC-Lyon}\right) - 1\right) \times 10^3$$
$$\delta^{68}Zn = \left(\left({}^{68}Zn/{}^{64}Zn_{sample}\right)/\left({}^{68}Zn/{}^{64}Zn_{JMC-Lyon}\right) - 1\right) \times 10^3$$

Due to a limited supply of the JMC-Lyon standard solution, samples were measured relative to AA-ETH standard offset from JMC-Lyon by −0.29 (±0.05, 2sd) ‰ for δ^{66}Zn (over two years of measurements and in good agreement with Archer et al., 2017). We corrected our measured values accordingly to report them relative to JMC-Lyon, as is widely accepted.

In addition, reference materials (UB-N serpentinite and JP-1 peridotite) were processed through columns and analyzed for δ^{66}Zn, δ^{68}Zn and δ^{65}Cu alongside samples. They gave accurate δ^{65}Cu values of 0.06 ± 0.05 ‰ and 0.06 ± 0.03 ‰, δ^{66}Zn values of 0.13 ± 0.01 ‰ and 0.32 ± 0.06 ‰, and δ^{68}Zn values of 0.31 ± 0.02 ‰ and 0.66 ± 0.1 ‰ for JP-1 (n = 4 for Cu, n = 2 for Zn) and UB-N (n = 6 for Cu, n = 4 for Zn), respectively, in agreement with previous studies (Bishop et al., 2012; Telus et al., 2012; Liu et al, 2015; Wang et al., 2017) (Table 1).

4. Results

The measured isotopic compositions of the MARK mantle rocks are reported in Fig. 3 and are given in Table 1. Regardless of the lithological group, our samples mostly display low δ^{56}Fe (−0.44 to 0.07 ± 0.03 ‰) compared to estimates of the primitive mantle (0.025 ± 0.025 ‰; Craddock et al., 2013; McCoy-West et al., 2018; Doucet et al., 2020). The MPs display the broadest range of isotopic compositions, possibly because of a greater number of samples analyzed in this group. They reach values as low as those measured in metasomatized peridotites in subcontinental and oceanic domains (Weyer and Ionov, 2007; Poitrasson et al., 2013; Zhao et al., 2015). SPs that underwent melt-rock interaction have the lowest δ^{56}Fe (−0.23 ± 0.03 ‰ and −0.39 ± 0.05 ‰) of this lithological group. δ^{65}Cu values range from −0.19 to 0.38 ± 0.04 ‰, and are centered around the primitive mantle composition (0.07 ± 0.1 ‰, Savage et al., 2015). One HPs has the lowest δ^{65}Cu value (−0.19 ± 0.02 ‰) but the second sample overlaps with the two other lithological groups (full range from −0.11 to 0.38 ± 0.04 ‰). δ^{65}Cu values of our sample suite both overlap Cu isotope compositions of common abyssal serpentinized peridotites and metasomatized (serpentinized) peridotites. It is noteworthy that δ^{65}Cu values of SPs can be heavier (up to 0.25 ± 0.05 ‰) than those of the MARK serpentinites reported by Debret et al. (2018). δ^{66}Zn values are heterogenous and range from −0.24 to 0.35 ± 0.04 ‰, values lower than those of the MARK and common abyssal serpentinites (Pons et al., 2011; Debret et al., 2018; Liu et al., 2019). MPs reach values as low as those measured in metasomatized peridotites and pyroxenites in subcontinental and oceanic domains (down to −0.44 ‰ and −0.33 ‰ for peridotite and pyroxenite, respectively; Pons et al., 2011; Wang et al., 2017; Sossi et al., 2018; Huang et al., 2019). HPs tend to have higher δ^{66}Zn values (0.27 to 0.34 ± 0.05 ‰) compared to the two other lithological groups for which δ^{66}Zn values overlap (−0.24 to 0.35 ± 0.04 ‰).

5. Discussion

The studied sample suite presents heterogenous Fe, Cu, Zn isotope compositions pointing to a complex magmato-hydrothermal history for the MARK mantle rocks. The lack of correlation between these isotopic systems (e.g., Supplementary Material – Figure S2) indicate that transition metal isotopes fractionate during different processes that need to be addressed individually. Here we investigate the contribution of (i) pre-existing mantle heterogeneity, (ii) kinetic isotope fractionation during melt-rock interaction, and (iii) fluid-rock interaction on the Fe, Cu and Zn isotopic variability of mantle rocks.

5.1. Mantle heterogeneity

Partial melting of mantle rocks to generate MORB-like melts and/or percolation of asthenospheric melts are two of the main processes that generate mantle heterogeneities, modifying the Al_2O_3/SiO_2 ratio of mantle rocks (e.g., Godard et al., 2008). These processes fractionate Fe isotopes (Weyer and Ionov, 2007), with apparent little effects on Cu and Zn isotopes (Savage et al., 2015; Sossi et al., 2018; Fang et al., 2022).

Iron isotopes fractionate during partial melting and leave residues with light δ^{56}Fe relative to melts (Weyer and Ionov, 2007). This results in a positive correlation between Al_2O_3/SiO_2 and δ^{56}Fe (melting arrow in Fig. 4B). Such a correlation is not observed in our samples that have variable $Fe_2O_3^t$ content and δ^{56}Fe values regardless of peridotite fertility (i.e., Al_2O_3/SiO_2; Fig. 4A). Although partial melting can account for Fe isotope variability in peridotites, this effect is limited as high degrees of melt extraction (>30 %) cannot generate strongly fractionated residues (< 0.1 ‰, Williams and Bizimis, 2014; Sossi and O'Neill, 2017; Dauphas et al., 2017). This suggests that partial melting cannot account for the Fe

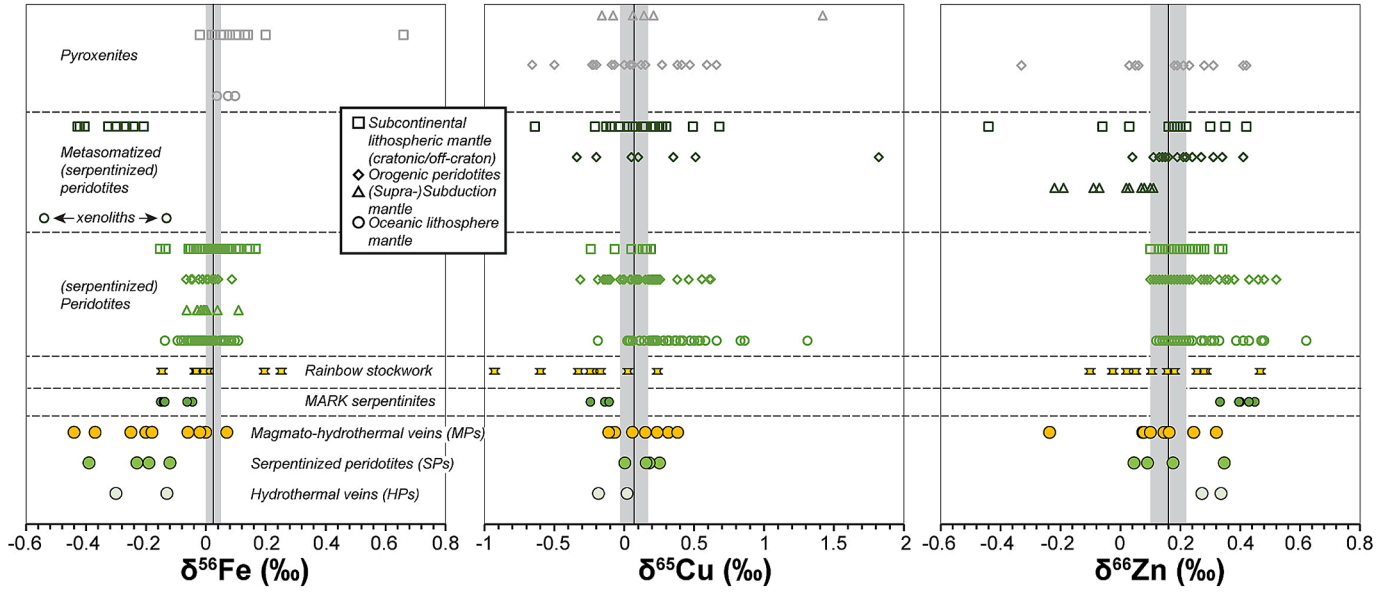

Fig. 3. δ^{56}Fe, δ^{65}Cu and δ^{66}Zn values in mantle rocks of the MARK area compared to ultramafic rocks from different settings. The vertical lines and grey boxes show the average and standard deviation of estimates of the primitive mantle (from Craddock et al., 2013; McCoy-West et al., 2018; Doucet et al., 2020 for Fe, Savage et al., 2015 for Cu and Sossi et al., 2018 for Zn). Data from the literature includes MARK serpentinites and Rainbow stockwork (Debret et al., 2018); (serpentinized) peridotites (Weyer and Ionov, 2007; Pons et al., 2011; Craddock et al., 2013; Poitrasson et al., 2013; Liu et al., 2015a,b; Zhao et al., 2015; Doucet et al., 2016; Huang et al., 2017a,b; Wang et al., 2017; Debret et al., 2018; Huang et al., 2018; Sossi et al., 2018; Huang et al., 2019; Liu et al., 2019); metasomatized (serpentinized) peridotites (Weyer and Ionov, 2007; Pons et al., 2011; Poitrasson et al., 2013; Liu et al., 2015a,b; Zhao et al., 2015; Wang et al., 2017; Huang et al., 2019) and pyroxenites (Ben Othman et al., 2006; Poitrasson et al., 2013; Zhao et al., 2017; Sossi et al., 2018; Huang et al., 2019; Zou et al., 2019; Kempton et al., 2022).

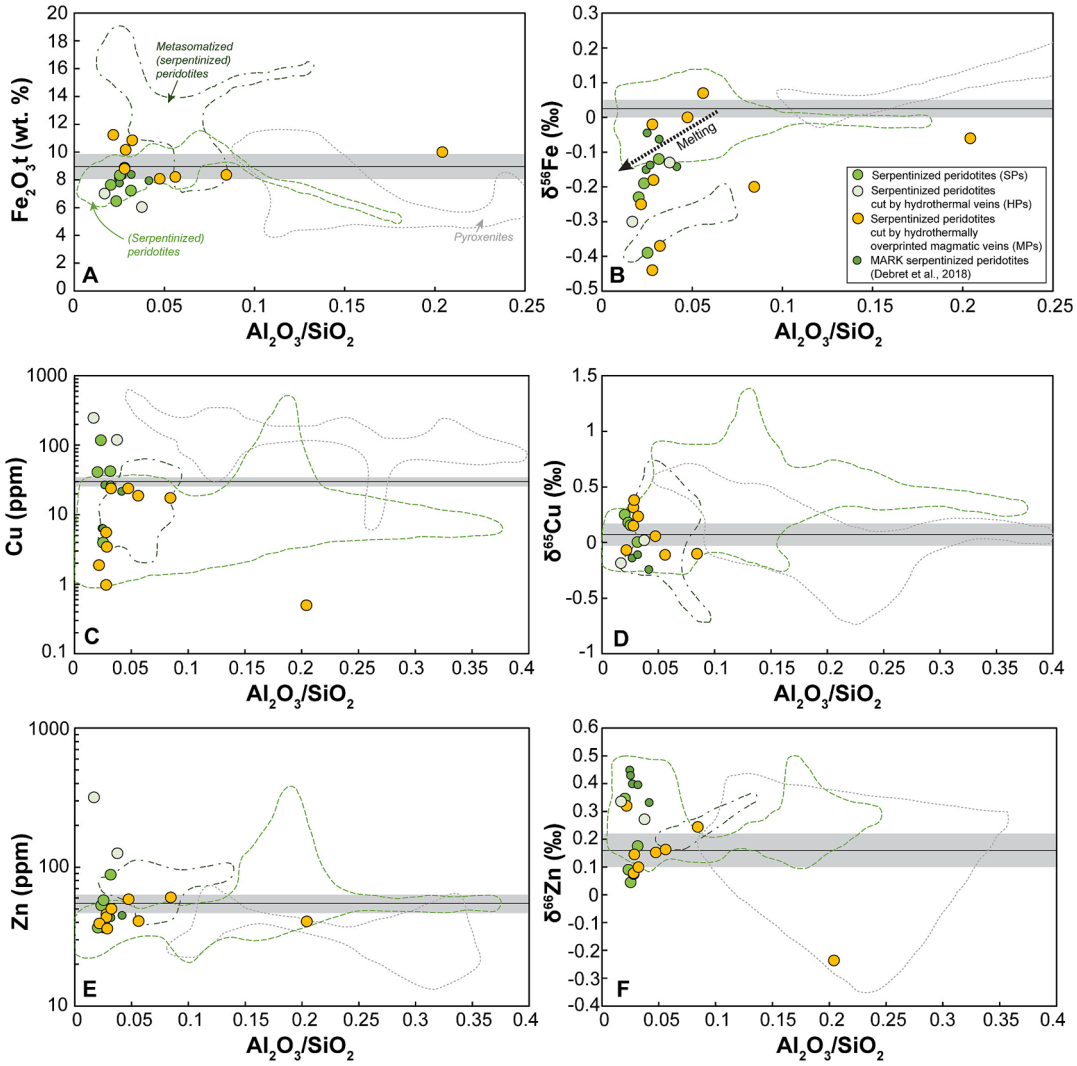

Fig. 4. Fe_2O_3, Cu and Zn concentrations and $\delta^{56}Fe$, $\delta^{65}Cu$ and $\delta^{66}Zn$ of mantle rocks of the MARK area vs a proxy for peridotite fertility (Al_2O_3/SiO_2). The melting trend is from Debret et al. (2018). The different lithological fields (i.e., serpentinized peridotites, metasomatized peridotites and pyroxenites) are built from data literature (see references in Fig. 3). Primitive mantle compositions are from McDonough and Sun (1995); Craddock et al., 2013; Savage et al., 2015; Sossi et al., 2018; McCoy-West et al., 2018 and Doucet et al., 2020.

isotopic variability observed here (−0.44 to 0.07 ± 0.03 ‰) The low $\delta^{56}Fe$ values are unlikely to be due to melt addition because melts display heavy $\delta^{56}Fe$ relative to primitive mantle (Fig. 4B, Craddock et al., 2013; McCoy-West et al., 2018; Doucet et al., 2020).

Most of MPs and SPs have $\delta^{65}Cu$ values (from −0.11 to 0.32 ± 0.04 ‰) that overlap the composition of the primitive mantle (0.07 ± 0.1 ‰) regardless of peridotite fertility (Fig. 4D). The $\delta^{65}Cu$ of MPs that extend the primitive mantle estimate composition might reflect magmatic material addition, as gabbroic rocks (full range between −1.14 ‰ to 0.87 ‰ for the South-West Indian Ridge gabbroic cumulates, Zou et al., 2024) and pyroxenite can have varying $\delta^{65}Cu$ (full range between −0.66 ‰ to 0.66 ‰ for the Balmuccia pyroxenites, Zou et al., 2019). At MARK, pyroxenite veining in peridotites has been documented based on petrographic observations (Cannat et al., 1995; Casey, 1997) and trace element compositions of serpentinized peridotites cut by hydrothermally altered magmatic veins (Coltat et al., 2023). However, as pyroxenitic (and gabbroic) melt is enriched in Cu relative to the primitive mantle, such melt addition in peridotite should increase the Cu content of the rock, while the reverse relation is observed (Fig. 4C). Therefore, mantle processes cannot account for the Cu element and isotopic variations at MARK.

Melt extraction during peridotite partial melting produces very little Zn isotope fractionation (< 0.08 ‰ between the residual peridotite and the melt; Sossi et al., 2018) and thus cannot explain the variable $\delta^{66}Zn$ values (−0.24 to 0.35 ± 0.04 ‰) of our samples compared to the primitive mantle (0.16 ± 0.06 ‰). As melts have higher Zn content and heavier $\delta^{66}Zn$ than the primitive mantle, melt addition in mantle rocks should result in a positive correlation between the Zn content and $\delta^{66}Zn$. This is not observed in our samples. On the other hand, variable Zn contents (15 to 70 ppm) and high $\delta^{66}Zn$ values have been measured in orogenic pyroxenites (up to 0.42 ‰; e.g., Sossi et al., 2018; Huang et al., 2019). At MARK, REE compositions of MPs support a scenario of pyroxenitic melt addition in mantle rocks (Coltat et al., 2023). Such melt addition may decrease the Zn content and increase the $\delta^{66}Zn$ values of percolated rocks relative to the primitive mantle composition (Zn = 55 ppm; $\delta^{66}Zn$ = 0.16 ± 0.06 ‰). This may explain the high $\delta^{66}Zn$ (0.35 ± 0.04 ‰ and 0.32 ± 0.05 ‰) and relatively low Zn content (37 and 39 ppm) measured in one SP and in one MP, respectively (Fig. 4E, F). However, this process fails to explain light $\delta^{66}Zn$ of MPs, as low as −0.24 ‰, pointing to another process.

5.2. Contribution of melt-rock interaction to kinetic isotope fractionation

Percolation of Fe-rich melts through mantle rocks creates a local

chemical gradient that promotes Mg-Fe interdiffusion between the melt and peridotite wall rock, leaving a metasomatized peridotite enriched in Fe (Weyer and Ionov, 2007; Zhao et al., 2015; 2017). Because light isotopes diffuse faster than heavy ones (Richter et al., 2009), the kinetic isotope fractionation induced by Fe-Mg diffusion should produce lighter δ^{56}Fe (i.e., preferential incorporation of ^{54}Fe) in the metasomatized peridotite compared to the melt. Most of MPs have lower δ^{56}Fe relative to worldwide serpentinized peridotites (Figs. 3, 4B) and have δ^{56}Fe values as low as those of Fe-rich peridotites (Zhao et al., 2015) and peridotites affected by melt metasomatism (i.e., metasomatized peridotites of Poitrasson et al., 2013; Fig. 3). Several numerical studies have calculated the extent of Fe kinetic isotope fractionation during melt-olivine interaction (Dauphas et al., 2010; Teng et al., 2011). Dauphas et al (2010) and Teng et al., (2011) predicted Fe isotope fractionation as high as 0.6 ‰ between olivine and melt, even considering low variations of Mg# between these. Such an isotopic range between olivine and melt encompasses the range of δ^{56}Fe values measured in MPs, suggesting that kinetic isotope fractionation during melt percolation might explain the Fe isotope variability measured in our samples.

Kinetic isotope fractionation can also account for important Zn isotope fractionation in peridotite interacting with Zn-rich melt (Wang et al., 2017; Huang et al., 2019; Fang et al., 2022). Considering the melt-olivine partition coefficient of Zn close to unity, diffusion gain of Zn in olivine is expected during melt percolation. Because of faster diffusion of ^{64}Zn over ^{66}Zn, this process results in neighboring peridotites having lower δ^{66}Zn than the primitive mantle, as recently observed in Fe-rich mantle rocks cut by pyroxenite veins (i.e., metasomatized peridotites, Fang et al., 2022). This process might explain low δ^{66}Zn values measured in MPs (down to −0.24 ‰).

We propose below that such a kinetic isotope fractionation occurs in the mantle rocks at MARK during melt percolation, as supported by high Fe and Zn contents measured in olivine at the contact with magmatic veins (up to 32.5 wt% FeO and 235 ppm Zn, Coltat et al., 2023) contrasting with residual mantle olivine (9.33 wt% FeO and ~ 56 ppm Zn, Coltat et al., 2023). To further test this hypothesis, we numerically simulate Fe and Zn isotope fractionation during the percolation of Fe-Zn-rich melts in mantle rocks at 1200 °C (Fig. 5). Instead of simple diffusion models in single spherical olivine-melt systems (i.e. where rim compositions are a fixed boundary conditions; e.g., Dauphas et al., 2010; Huang et al., 2018), we here consider the percolation process in a transport situation. To that end, we use a mass-balanced percolation-diffusion model (following the procedure of equations 1 to 4 described in Tilhac et al., 2023) consisting of a 1-D column made of a porous aggregate of spherical minerals. Hence, not only the kinetic fractionation associated with the diffusional gain of Fe and Zn is simulated, but also the diffusional loss from the melt as it percolates away from its source (e.g., a dyke) into the peridotite. The peridotite is here approximated as a matrix of olivine, which is a reasonable approximation considering the high modal abundance of primary olivine in MARK mantle rocks (> 80 %) suggesting that the whole-rock Fe-Zn budget is dominated by olivine. For the model, the kinetic isotope fractionation factors (β_{Zn} and β_{Fe}) in olivine that account for the slightly different diffusion coefficient of two different isotopes (see equation 3 in Huang et al., 2018) was set to 0.05 as proposed in previous studies (Dauphas et al., 2010; Huang et al., 2018). The different input and model parameters are listed in Table S1.

The model simulates temporal variations in the olivine diffusion profiles as a function of the position with respect to the melt source. For simplicity, we here only discuss the results obtained during 100 years near the contact with the ascending melts. The model predicts that the diffusional gain of Fe and Zn produces i) a strong isotope fractionation up to −0.6 ‰ and −0.33 ‰ for δ^{56}Fe and δ^{66}Zn, respectively (Fig. 5) and ii) the melt exhibits a transient enrichment (until the olivine is fully re-equilibrated) in heavy isotope due the loss of ^{54}Fe and ^{64}Zn and display high δ^{56}Fe and δ^{66}Zn values up to 0.32 ‰ and 0.47 ‰, respectively (Fig. 5). The combination of these competing effects results in a strong isotopic variability in olivine (grey fields in Fig. 5), ranging from variously low δ^{56}Fe and δ^{66}Zn throughout the grains to isotopically heavier rims, which essentially overlaps the whole range of isotope compositions measured in MPs at MARK. We conclude that Fe and Zn kinetic isotope fractionation during the ascent of Fe-Zn-rich melts result in the formation of metasomatized peridotites having lower δ^{56}Fe and δ^{66}Zn than the upper mantle from which they originally derive (i.e., δ^{56}Fe = 0.025 ± 0.025 ‰, Craddock et al., 2013; δ^{66}Zn = 0.16 ± 0.06 ‰; Sossi et al., 2018). High δ^{56}Fe and δ^{66}Zn values (samples 920D-4R-1, 80–81 cm and 920D-16R-7, 19–22 cm; Table 1) may reflect the mixing, in variable proportions, of isotopically heavy melts and light mantle rocks.

5.3. Metal behavior during fluid-rock interaction

At MARK, the increase of Cu and Zn contents with Rb/Nb in HPs indicates metal mobility during fluid-rock interaction (Fig. 6). In HPs, Cu and Zn are mostly scavenged by hydrothermal sulfide and in less extent serpentine (Fig. S3) indicating formation from a hydrothermal fluid enriched in S, Cu and Zn interacting with mantle rocks. No systematic metal depletion nor addition are observed in SPs, suggesting that serpentinization only has minor (local) effect on metal mobility. MPs have low Cu content (0.5–23.9 ppm), while their Zn content remains fairly constant (36–60 ppm) at varying Rb/Nb. This suggests Cu (and Rb) leaching during HT (> 350 °C) hydrothermal alteration, while Zn remains relatively unsensitive (Coltat et al., 2023). Hence, the metal concentrations of our samples point to two different processes, namely i)

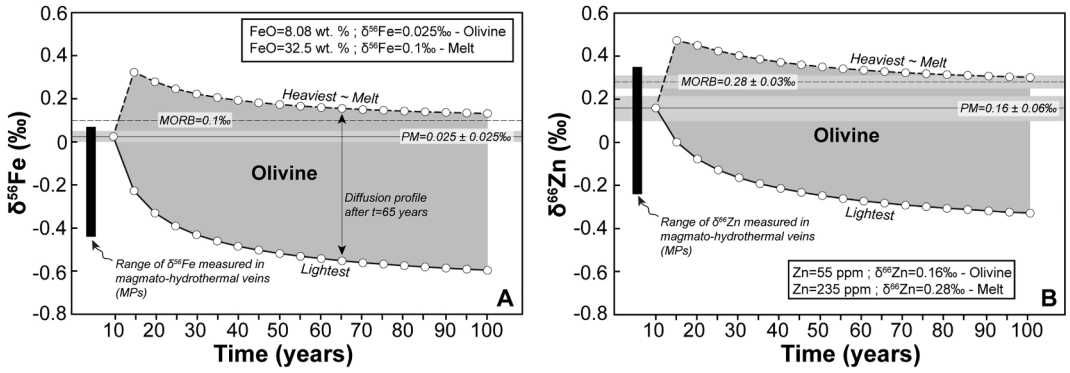

Fig. 5. Modeled kinetic (diffusive) fractionation of δ^{56}Fe and δ^{66}Zn in olivine during melt percolation in olivine-dominated mantle rocks. At each time increment, the two dots correspond either to the minimum (kinetic isotope fractionation) or maximum (heavy isotope enrichment in melt) isotope fractionation predicted by numerical modeling for a given isotopic profile in olivine. The grey fields labelled "olivine" show the full ranges of Fe and Zn isotope compositions of olivine percolated by the melt. The Fe and Zn elemental and isotopic compositions given in boxes represent the starting compositions of the olivine column and the melt that percolates it.

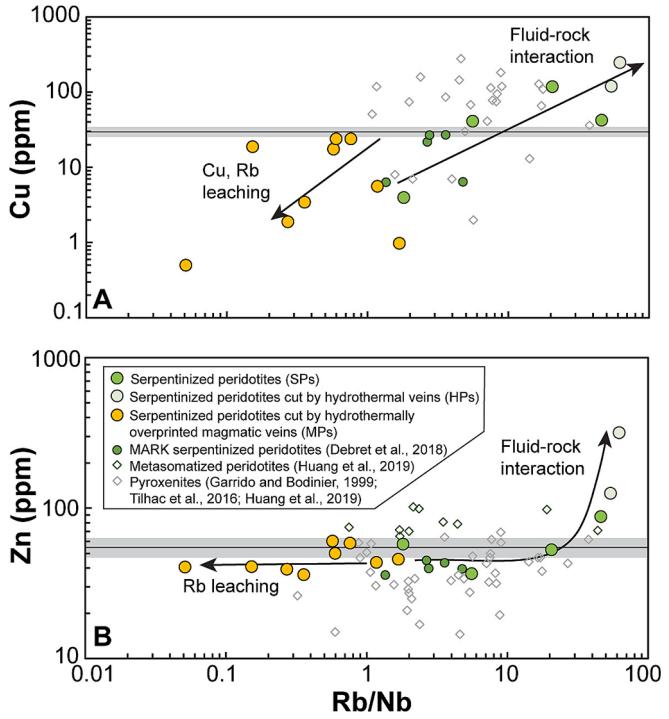

Fig. 6. (A) Cu and (B) Zn concentrations of mantle rocks of the MARK area vs Rb/Nb ratio, a proxy for fluid-rock interaction. The primitive mantle compositions (grey bars) are from McDonough and Sun (1995).

Cu leaching from primary sulfides/oxides/silicates during hydrothermal alteration of MPs and ii) hydrothermal veining and formation of HPs from a metal- and sulfur-rich fluid interacting with serpentinized peridotite. Below, we investigate these two processes through geochemical modeling to constrain the physico-chemical conditions during fluid-rock interaction.

5.3.1. *Cu leaching during HT hydrothermalism*

We use a simple Rayleigh distillation model to predict Cu leaching and transport as different complexes in fluid during the dissolution of sulfides, oxides and Cu-bearing silicates in MPs. To that end, we assume that the element and isotopic behavior of Cu in whole rock can be approximated to that of chalcopyrite (for sulfides), cuprite (for oxides) and Cu-bearing enstatite (for silicates; i.e., β-factor). This approach has been successfully used to model Zn leaching during serpentinization of mantle rocks (Debret et al., 2018). Fig. 7 shows the model for Cu leaching by chlorine-bearing fluids ($CuCl(H_2O)_4^+$); additional models are shown in Figure S4. We used the ab initio calculations compiled in Moynier et al. (2017) for [$CuCl_3(H_2O)^-$] complex in fluids (Fujii et al., 2013) and those of Liu et al. (2021) for chalcopyrite ($CuFeS_2$), cuprite (CuO) and Cu-bearing enstatite ($Mg_{31/16}Cu_{1/16}Si_2O_6$). We run isotopic distillation models at 100, 300, 450 and 600 °C. Based on petrographic observations, we assume the starting composition of the MPs to be a 1:1 peridotite-pyroxenite mixture. Considering a primitive mantle starting composition would yield isotopic dilution trends that fail to reproduce the measured compositions at investigated temperatures (Fig. S4). The $\delta^{65}Cu$ evolution of MPs during hydrothermal alteration is then modeled, according to the following equations:

$$10^3 ln(\alpha_{fluid-mineral}) = 10^3 ln(\beta_{fluid}) - 10^3 ln(\beta_{mineral})$$
$$\delta^{65}Cu_{Final} = (1000 + \delta^{65}Cu_{Initial}) \times (F^{(\alpha-1)} - 1) + \delta^{65}Cu_{Initial}$$

where α is the fractionation factor between sulfides, oxides or Cu-bearing silicates and a fluid phase complexing Cu as [$CuCl_3(H_2O)^-$] at 100, 300, 450 or 600 °C; β is the reduced partition function ratio of isotopologues that allow the obtention of the equilibrium constant of an isotopic exchange reaction (e.g., Moynier et al., 2017); F is the fraction of Cu remaining in the rock, ranging from 1 (unreacted) to 0 (all of Cu lost to the fluid phase); $\delta^{65}Cu^{Initial}$ was set to a value corresponding to as the peridotite-pyroxenite mixture in 1:1 proportion (0.12 ± 0.1 ‰; e.g., Ben Othman et al., 2006; Savage et al., 2015; Zou et al., 2019; Kempton et al., 2022).

Our model predicts that at any considered temperature, the dissolution of Cu-bearing enstatite is accompanied with important Cu isotope fractionation (up to 2.5 ‰) that fails to reproduce the isotopic variability observed in our samples. At 100 and 300 °C, the dissolution of sulfide leaves a residual rock with low $\delta^{65}Cu$ values that fails to reproduce the $\delta^{65}Cu$ values of our samples (Fig. 7, Fig. A4), while oxide dissolution at 300 °C produces limited Cu isotope fractionation that cannot explain the high $\delta^{65}Cu$ values. At temperatures > 450 °C, cuprite dissolution leaves a residual rock with high $\delta^{65}Cu$ values that are close to the highest compositions measured in our samples. More discriminant is chalcopyrite dissolution; at 450 °C and 600 °C it is accompanied with moderate Cu isotope fractionation towards, respectively, low $\delta^{65}Cu$ and high $\delta^{65}Cu$ values, reproducing the range of $\delta^{65}Cu$ measured in MPs. Therefore, the Cu elemental and isotope compositions of MPs may be explained by Cu leaching during sulfide dissolution at temperatures of ~ 450–600 °C. This scenario is plausible considering that Cu is mostly sourced in sulfides in magmatic and mantle rocks (e.g., Luguet et al., 2001; Liu et al., 2015a,b; Patten et al., 2016). This range overlaps with the ~ 420–830 °C temperature range calculated for hydrothermal alteration based on Ti-thermometry in amphibole present in MPs and one altered gabbro at MARK (Coltat et al., 2023). Alternatively,

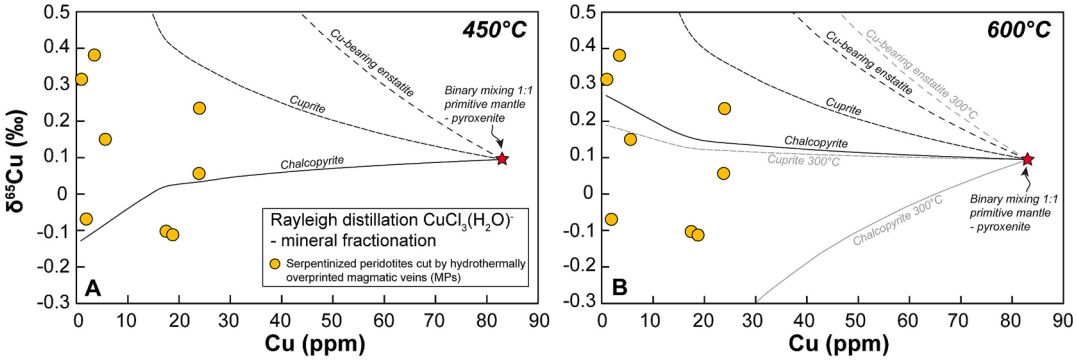

Fig. 7. Modeled and measured of $\delta^{65}Cu$ (‰) vs Cu (ppm) of serpentinized peridotites cut by hydrothermally overprinted magmatic veins at MARK. Modeled compositions are obtained from leaching of $CuCl_3(H_2O)^-$ during the dissolution of Cu-bearing enstatite, chalcopyrite and cuprite at temperatures of 450 °C (A) and 600 °C (B). In (B) are also displayed the modeled Cu element and isotope compositions at 300 °C considering the same reacting minerals (grey lines). The initial Cu content and isotope composition (red star) is set to as a 1:1 mixture of peridotite-pyroxenite (0.095 ± 0.1 ‰; 83 ppm Cu; e.g., Frey, 1980; Garrido and Bodinier, 1999; Ben Othman et al., 2006; Savage et al., 2015; Tilhac et al., 2016; Huang et al., 2019; Zou et al., 2019; Kempton et al., 2022).

considering hydrothermal alteration to occur at 450 °C, we cannot rule out that Cu might also derive from both sulfide and oxide dissolution. Indeed, Fe(−Ti) oxides in pyroxenites can be enriched in Cu (up to 3.66 wt%), significantly accounting for the Cu whole rock budget (Kempton et al, 2022). Finally, at such HT condition (>450 °C), Cu isotope fractionation predicted by Rayleigh distillation models is roughly similar regardless of the nature of Cu-bearing complexes in hydrothermal fluid (e.g., $CuCl(H_2O)_4^+$, $Cu(HS)_2(H_2O)_3$, $CuHS(H_2O)_4^+$, $CuOH(H_2O)_4^+$, $CuCO_3(H_2O)_2$; Fig. S4). Hence, the precise nature of species complexing Cu in hydrothermal fluids cannot be constrained solely from our results.

5.3.2. *Hydrothermal veining in serpentinized peridotites*

Petrographic evidence constrains HPs formation during or after serpentinization of mantle rocks (Coltat et al., 2023). From the above Rayleigh distillation models, we observe that Cu is leached, at HT conditions, during the dissolution of magmatic and mantle sulfide and possibly oxide. We do not have evidence to constrain the Zn sources. In mantle rocks, spinel is the main source of Zn and is commonly altered during serpentinization of mantle rocks (Burkhard, 1993), while silicates can account for the Zn budget in lesser extents (e.g., Wang et al., 2017; Fang et al., 2022; Lin et al., 2023). Seawater circulation and leaching of mantle and magmatic sulfides and oxides is expected to produce Cu and Zn-rich, high chlorinity and HS-bearing fluids (Alt and Shanks, 2003; Debret et al., 2018), possibly similar to those from which hydrothermal vein form in HPs.

We model the interaction between serpentinized peridotites and such a metal-, chlorine- and HS-rich hydrothermal fluid by using different fractions of these two components. We calculate the δ^{65}Cu and δ^{66}Zn values of the hydrothermal fluid using various proportions of pyroxenite (0, 50 and 100 %). Copper is expected to entirely derive from chalcopyrite, and Zn from spinel. To test a potential source of Zn from magmatic sulfides and mantle silicates, we also model Zn leaching from sphalerite and hemimorphite ($Zn_4Si_2O_7(OH)_2{\cdot}H_2O$), respectively. This defines a large range of fluid compositions from which ab initio calculations exist for Cu ($CuCl(H_2O)_4^+$; $CuCl_3(H_2O)^-$; $CuHS(H_2O)_4^+$; $Cu(HS)_2(H_2O)_3$; $CuCO_3(H_2O)_2$; $CuOH(H_2O)_4^+$; Fujii et al., 2013; Moynier et al., 2017) and Zn ($ZnCl(H_2O)_5^+$; $ZnCl_4^{2-}$; $Zn(HS)_3(H_2O)_2^-$; $Zn(HS)_4^{2-}$; $ZnHCO_3(H_2O)_5^+$; $Zn(OH)_2(H2O)_4$; Fujii et al., 2011; 2013; Moynier et al., 2017). We set the reaction progress to an average value of 0.5, meaning that the reacting rocks lose half of their metal budget to the hydrothermal fluid. This value accounts for the remaining magmatic sulfides and unaltered mantle spinel in magmatic and mantle rocks of the MARK area, respectively. This fluid mixes with serpentinized peridotites which Cu and Zn elemental and isotope compositions are set to the average values of SPs measured in this study ([Cu] = 51.3 ppm; δ^{65}Cu = 0.15 ‰, [Zn] = 59 ppm; δ^{66}Zn = 0.16 ‰). The HPs can be considered as a mixture between the serpentinized peridotites and mantle-derived fluids:

$$\delta^{65}Cu_{mixture} = \left(N_a\delta^{65}Cu_a + N_b\delta^{65}Cu_b\right)/(N_a + N_b)$$
$$\delta^{66}Zn_{mixture} = \left(N_a\delta^{66}Zn_a + N_b\delta^{66}Zn_b\right)/(N_a + N_b)$$

where N_a and N_b are the amounts of Cu or Zn added to the rock during progressive fluid-rock interaction and the initial Cu or Zn contents of the serpentinized peridotite, respectively. δ^{65}Cu and δ^{66}Zn values of HPs can be explained by the mixture of chalcopyrite-derived fluids (for Cu) and spinel-derived fluids (for Zn) and serpentinized peridotites at temperatures of ~ 300 °C (Fig. 8). Both Cl-bearing and HS-bearing complexes can produce the measured δ^{65}Cu and δ^{66}Zn values of HPs, hindering the determination of the metal-bearing complexes that are transported by the hydrothermal fluid. The most probable Cu-bearing complexes are $CuCl_3(H_2O)^-$, Cu(HS) and $Cu(HS)_2$ and Zn-bearing complexes are $ZnCl(H_2O)_5^+$ and $Zn(HS)_3(H_2O)_2^-$. Sphalerite dissolution probably has a negligible effect on the Zn budget because a fluid in equilibrium with sphalerite yields lighter δ^{66}Zn than that of a spinel-derived fluid (Fig. 8). However, dissolution of Zn-bearing silicates during serpentinization may indeed have accounted for part of the Zn budget. This is supported by our geochemical modeling that predict that a HS- and/or Cl-bearing fluid in equilibrium with hemimorphite mixing with serpentinite would yield Zn isotope compositions close to those measured (Fig. S5C). In agreement with that, at similar temperatures (~311 °C), experiments showed that spinel is efficiently altered during serpentinization and that associated Al and Cr release would enhance the kinetic of mantle olivine dissolution (Huang et al., 2017a,b). Finally, a Cl- or HS-bearing fluid reacting with the rock at 100 °C, at the same F = 0.5, would produce δ^{65}Cu values lower than those measured for HPs (Fig. 8). Note that δ^{65}Cu and δ^{66}Zn values in carbonate- ($CuCO_3(H_2O)_2$ and $ZnHCO_3(H_2O)_5^+$) and hydroxyl-bearing fluids ($CuOH(H_2O)^{4+}$ and $Zn(OH)_2(H2O)_4$) were also modeled and both predict lower δ^{65}Cu and δ^{66}Zn than those measured with Cl- and HS-bearing fluids (Fig. S5A, B).

5.4. *Isotopic variability of the oceanic lithospheric mantle recorded by magmato-hydrothermal processes during mantle exhumation*

Tectonically exhumed mantle rocks make up to 10–25 % of the Earth's seafloor, reaching up to ~ 50 % in certain areas like the Northern Mid-Atlantic Ridge (Escartín et al., 2008) and the Central Indian Ridge (Pak et al., 2017). Only a few studies have investigated the magmato-hydrothermal processes in the oceanic mantle using Fe, Cu, Zn isotopes (Craddock et al., 2013; Debret et al., 2018; Liu et al., 2019), focusing mainly on dredge/dive samples where seafloor weathering is significant. In this study, which examines drilled serpentinized peridotites of the MARK area, we demonstrate that the oceanic lithospheric mantle records contrasted Fe, Cu, and Zn element and isotopic compositions on a relatively small scale (< 200 m), primarily controlled by magmatic and hydrothermal processes during mantle exhumation. Consistent with previous studies (e.g., Sossi et al., 2018; Fang et al.,

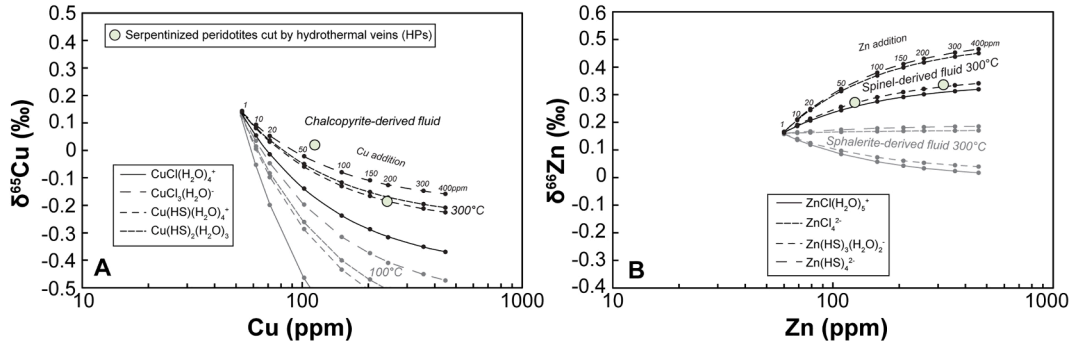

Fig. 8. Plots of the δ^{65}Cu and δ^{66}Zn versus Cu and Zn concentrations, respectively, in the serpentinized peridotites cut by hydrothermal veins. The black lines represent the modeled (A) addition of Cu by dissolution of $CuCl(H_2O)_4^+$; $CuCl_3(H_2O)^-$; Cu(HS); $Cu(HS)_2$ at temperatures of 100 and 300 °C and (B) addition of Zn by dissolution of $ZnCl(H_2O)_5^+$; $ZnCl_4^{2-}$; $Zn(HS)_3(H_2O)_2^-$; $Zn(HS)_4^{2-}$ either deriving from oxide (spinel) or sulfide (sphalerite).

2022), it appears that mantle heterogeneity does not predominantly control the isotopic heterogeneity. Instead, isotopic differences in oceanic lithospheric mantle can be attributed to kinetic isotope fractionation during melt-rock interaction or fluid-rock interaction under varying thermal conditions. This raises the question of whether the magmato-hydrothermal processes responsible for isotopic variability at MARK might be widespread across mantle-dominated MOR environments. Consequently, the oceanic lithospheric mantle at intermediate to ultraslow-spreading ridges could be isotopically heterogenous.

At MARK, following textural and geochemical observations and data, magmatic veins and dykes form at the base of the lithosphere during early mantle exhumation (see Fig. 14 of Cannat et al., 1997). Cannat et al. (1997) proposed that melts crystallize in hot mantle rocks near the melt solidus temperature (~860 ± 30 °C). At 15°N, an oceanic core complex drilled along the MAR revealed even higher thermal conditions for magmatic impregnation of mantle rocks (~1100 °C; ODP Leg 209; Kelemen et al., 2007). At these temperatures, element inter-diffusion between melt and rock occurs rapidly (several years to several ky; Dauphas et al., 2010) compared to long-lived tectono-magmatic processes related to mantle exhumation (100 ky to several My; Grimes et al., 2008; Escartín and Olive, 2022). At Site 920 at MARK, Cannat et al. (1997) estimated that magmatic intrusions only make up 4 % of the total rock volume. However, magmatic rocks may represent a more substantial part of oceanic core complexes. This is supported by deep drill holes in gabbroic rocks at the Atlantis Massif (Hole U1309D, 30°N, MAR; Blackman et al., 2006) and the Atlantis Bank (Hole 735B, 57°E, South West Indian Ridge, Dick et al., 2019) and lithological estimations made at 15°N yielding ~ 20–40 % of magmatic rocks intruding mantle rocks (Kelemen et al., 2007). These findings align with results from the recent IODP Exp 399, which recovered ~ 30 % of magmatic rocks along a 1268 m section of mantle rocks at the Atlantis Massif (Lissenberg et al., 2024). Considering the timing of magmatic processes and volume of magmatic rocks formed in the oceanic lithosphere mantle, we infer that significant diffusion-induced Fe and Zn isotope fractionation can be recorded in deep mantle rocks worldwide before mantle exhumation at the seafloor. This is supported by the low δ^{56}Fe measured in oceanic metasomatized mantle xenoliths of the Kerguelen archipelago (down to −0.54 ‰, Fig. 3; Poitrasson et al., 2013). As mantle and magmatic rocks are progressively exhumed and transported from the lithosphere base, long-lived (Grimes et al., 2008) magmatic processes sustain melt injection in newly-formed hot lithospheric mantle rocks, further generating isotopic variability. This may eventually expend to the entire oceanic lithospheric mantle.

During mantle exhumation and cooling, downward seawater circulations interact with the exhuming rocks, producing various hydrothermal alterations (Table 1) that lead to Cu (and Zn) isotope fractionation in hydrothermal veins, while locally preserving the Fe isotope compositions inherited from deep melt-rock interaction. Coltat et al. (2023) showed, through petrographic and geochemical tracing, that mantle and magmatic rocks at MARK experienced continuous fluid-rock interaction at varying thermal regimes, from sub-solidus conditions (< 850 °C) to lower temperatures during serpentinization (< 400 °C). These varying thermal regimes during fluid-rock interaction are supported by the Cu and Zn isotopic compositions of MARK mantle rocks. This suggests a long hydrothermal history, possibly occurring at different structural positions during mantle exhumation. Metamorphic conditions from upper amphibolite (> 650 °C) to sub-greenschist facies (< 250 °C) were reported in altered mantle and magmatic rocks drilled at oceanic core complexes (Kelemen et al., 2007; Früh-Green et al., 2018; Dick et al., 2019; Lissenberg et al., 2024), suggesting comparable hydrothermal histories as for MARK. Therefore, despite a general lack of Fe, Cu and Zn isotope data of drilled rocks at oceanic core complexes, it is reasonable to think that hydrothermal processes account for similar isotopic variability in these settings. If this hypothesis holds true, it means that fluid-rock interaction might primarily control the Cu budget and isotope composition of the oceanic lithospheric mantle, a theory that needs further testing.

6. Conclusions

Serpentinized peridotites drilled at the Mid-Atlantic Ridge Kane area offer an opportunity to unravel the magmatic and hydrothermal processes with regard to metal mobility during mantle exhumation. We conducted Fe, Cu and Zn isotope analyses on mantle rocks to constrain these processes. As a main outcome, metals show contrasted behaviors regarding of magmatic or hydrothermal processes. We show that Fe and Zn isotopes are sensitive to kinetic isotope fractionation during melt-rock interaction. This increased isotopic heterogeneity to both lighter and heavier isotope compositions (δ^{56}Fe from −0.44 to 0.07 ± 0.03 ‰; δ^{66}Zn from −0.24 to 0.32 ± 0.04 ‰) expending the range around the predictive unaltered composition of the primitive mantle(0.025 ± 0.025 ‰ and 0.16 ± 0.06 ‰, respectively). This process promotes large isotope heterogeneity in mantle rocks, exceeding the range expected during mantle processes (i.e., partial melting, mantle heterogeneity through melt fertilization). Hence, one may be careful at investigating mantle source heterogeneity using Fe and Zn isotope systematics. Copper is sensitive to hydrothermal processes at varying thermal conditions. It is leached during HT hydrothermal alteration (~ 450–600 °C), producing variable δ^{65}Cu depending on the Cu source (sulfide and oxide), while Cu and Zn are efficiently mobilized during LT (300 °C) hydrothermal circulations in Cl- and/or HS-bearing fluids possibly genetically linked to serpentinization. Finally, our study reveals that transition metal isotopes, namely Fe, Cu and Zn, can bring valuable information on both magmatic and hydrothermal processes in mantle rocks over a wide range of temperatures that is relevant for the tectono-magmatic evolution of spreading centers.

CRediT authorship contribution statement

R. Coltat: Writing – original draft, Methodology, Investigation, Funding acquisition, Conceptualization. **B. Debret:** Writing – review & editing, Methodology, Investigation, Funding acquisition, Validation. **R. Tilhac:** Writing – review & editing, Software, Methodology. **M. Andreani:** Writing – review & editing, Supervision. **C.G.C. Patten:** Writing – review & editing. **M. Godard:** Writing – review & editing. **J. Escartín:** Writing – review & editing, Supervision.

Declaration of competing interest

The authors declare that they have no known competing financial interests or personal relationships that could have appeared to influence the work reported in this paper.

Acknowledgments

This work was funded through IODP-France (OPE-2021-93), CNRS-INSU grants from the Institut National des Sciences de l'Univers (INSU), the Agence Nationale de la Recherche (ANR) CARBioNic "ANR-22-CE49-0001-01". R. Coltat and R. Tilhac acknowledge "Juan de la Cierva" Fellowships (FJC2021-047190-I and IJC2020-044739-I, respectively), funded by MCIN/AEI/10.13039/501100011033 with EU Next Generation Funds and funding from project PID2022-136471NB-C21 "The role of ultramafic rocks and related rocks in the sulfur and water cycles and their implications for the redox state of subduction zones (RUSTED)", funded by MCIN/AEI/10.13039/501100011033 and by the ESF + .. Part of this work was also supported by IPGP multidisciplinary program PARI, and by Region Ile-de-France SESAME grants no. 12015908 and EX047016. The authors gratefully thank D. Rigoussen for his help to acquire Fe, Cu an Zn isotopic data.

Appendix A. Supplementary material

Supplementary material to this article can be found online at https://doi.org/10.1016/j.gca.2024.11.013.

References

Agrinier, P., Cannat, M., 1997. Oxygen-isotope constraints on serpentinization processes in ultramafic rocks from the Mid-Atlantic Ridge (23°N). In: Proceedings of the Ocean Drilling Program, Scientific Results 153, 381–388.

Alt, J.C., Shanks, W.C., 2003. Serpentinization of abyssal peridotites from the MARK area, Mid-Atlantic Ridge: Sulfur geochemistry and reaction modeling. Geochim. Cosmochim. Acta 67, 641–653.

Andreani, M., Mével, C., Boullier, A.-M., Escartín, J., 2007. Dynamic control on serpentine crystallization in veins: Constraints on hydration processes in oceanic peridotites. Geochem. Geophys. Geosyst. 8, 24.

Archer, C., Andersen, M.B., Cloquet, C., Conway, T.M., Dong, S., Ellwood, M., Moore, R., Nelson, J., Rehkämper, M., Rouxel, O., 2017. Inter-calibration of a proposed new primary reference standard AA-ETH Zn for zinc isotopic analysis. J. Anal. At. Spectrom 32, 415–419.

Beard, B.L., Johnson, C.M., Skulan, J.L., Nealson, K.H., Cox, L., Sun, H., 2003. Application of Fe isotopes to tracing the geochemical and biological cycling of Fe. Chem. Geol. 195, 87–117.

Ben Othman, D., Luck, J.M., Bodinier, J.L., Arndt, N.T., Albarede, F., 2006. Cu–Zn isotopic variations in the Earth's mantle. Geochim. Cosmochim. Acta 18, A46.

Bishop, M.C., Moynier, F., Weinstein, C., Fraboulet, J.-G., Wang, K., Foriel, J., 2012. The Cu isotopic composition of iron meteorites. Meteorit. Planet. Sci. 47, 268–276.

Blackman, D.K., Ildefonse, B., John, B.E., Ohara, Y., Miller, D.J., MacLeod, C.J., Scientists, and the expedition 304/305, 2006. Expedition 304/305 summary. Proceedings of the IODP, 304/305 304.

Burkhard, D.J.M., 1993. Accessory chromium spinels: Their coexistence and alteration in serpentinites. Geochim. Cosmochim. Acta 57, 1297–1306.

Cannat, M., Chatin, F., Whitechurch, H., Ceuleneer, G., 1997. Gabbroic rocks trapped in the upper mantle at the Mid-Atlantic Ridge, in. Proc. Ocean Drill. Program Sci. Results. 11, 243–264.

Cannat, M., Karson, J. a., Miller, D.J., Party, S.S., 1995. ODP Leg 153 MARK Initial Report. Proceedings ODP Initial Reports 153.

Coltat, R., Andreani, M., Patten, C.G.C., Godard, M., Debret, B., Escartin, J., 2023. Origin of Fe-Ca-Metasomatism in Exhumed Mantle Rocks at the MARK Area (23°N, ODP Leg 153) and Implications on the Formation of Ultramafic-Hosted Seafloor Massive Sulfide Deposits. Geochem. Geophys. Geosyst. 24 e2023GC010894.

Craddock, P.R., Warren, J.M., Dauphas, N., 2013. Abyssal peridotites reveal the near-chondritic Fe isotopic composition of the Earth. Earth Planet. Sci. Lett. 365, 63–76.

Dauphas, N., Teng, F.-Z., Arndt, N.T., 2010. Magnesium and iron isotopes in 2.7 Ga Alexo komatiites: Mantle signatures, no evidence for Soret diffusion, and identification of diffusive transport in zoned olivine. Geochim. Cosmochim. Acta 74, 3274–3291.

Dauphas, N., John, S.G., Rouxel, O., 2017. Iron Isotope Systematics. Rev. Mineral. Geochem. 82, 415–510.

Debret, B., Beunon, H., Mattielli, N., Andreani, M., Ribeiro da Costa, I., Escartín, J., 2018. Ore component mobility, Trannsport and mineralization at Mid-Oceanic ridges: a stable isotopes (Zn, Cu and Fe) study of the Rainbow massif (Mid-Atlantic Ridge 36°14′N). Earth Planet. Sci. Lett. 503, 170–180.

Debret, B., Garrido, C.J., Pons, M.-L., Bouilhol, P., Inglis, E., Sánchez-Vizcaíno, V.L., Williams, H., 2021. Iron and zinc stable isotope evidence for open-system high-pressure dehydration of antigorite serpentinite in subduction zones. Geochim. Cosmochim. Acta 296, 210–225.

Debret, B., Sverjensky, D.A., 2017. Highly oxidising fluids generated during serpentinite breakdown in subduction zones. Sci. Rep. 7, 10351.

Dick, H.J.B., Tivey, M.A., Tucholke, B.E., 2008. Plutonic foundation of a slow-spreading ridge segment: Oceanic core complex at Kane Megamullion, 23°30′N, 45°20′W. Geochemistry, Geophysics, Geosystems, p. 9.

Dick, H.J.B., Kvassnes, A.J.S., Robinson, P.T., MacLeod, C.J., Kinoshita, H., 2019. The Atlantis Bank Gabbro Massif, Southwest Indian Ridge. Prog Earth Planet Sci 6, 1–70.

Doucet, L.S., Mattielli, N., Ionov, D.A., Debouge, W., Golovin, A.V., 2016. Zn isotopic heterogeneity in the mantle: A melting control? Earth Planet. Sci. Lett. 451, 232–240.

Doucet, L.S., Laurent, O., Ionov, D.A., Mattielli, N., Debaille, V., Debouge, W., 2020. Archean lithospheric differentiation: Insights from Fe and Zn isotopes. Geology 48, 1028–1032.

Escartín, J., Olive, J.A., 2022. Mid-Ocean Ridges and Their Geomorphological Features. Treatise on Geomorphology, Journal, pp. 847–881.

Escartín, J., Smith, D.K., Cann, J., Schouten, H., Langmuir, C.H., Escrig, S., 2008. Central role of detachment faults in accretion of slow-spreading oceanic lithosphere. Nature 455, 790–794.

Fang, S.-B., Huang, J., Zhang, X.-C., Ionov, D.A., Zhao, Z.-F., Huang, F., 2022. Zinc isotope fractionation in mantle rocks and minerals, and a revised δ66Zn value for the Bulk Silicate Earth. Geochim. Cosmochim. Acta 338, 79–92.

Fouquet, Y., Cambon, P., Etoubleau, J., Charlou, J.L., Ondréas, H., Barriga, F.J.A.S., Cherkashov, G., Semkova, T., Poroshina, I., Bohn, M., Donval, J.P., Henry, K., Murphy, P., Rouxel, O., 2010. Geodiversity of Hydrothermal Processes Along the Mid-Atlantic Ridge and Ultramafic-Hosted Mineralization: A New Type of Oceanic Cu-Zn-Co-Au Volcanogenic Massive Sulfide Deposit. Geophys. Monogr. Ser. 188, 321–367.

Früh-Green, G.L., Orcutt, B.N., Rouméjon, S., Lilley, M.D., Morono, Y., Cotterill, C., Green, S., Escartin, J., John, B.E., McCaig, A.M., Cannat, M., Ménez, B., Schwarzenbach, E.M., Williams, M.J., Morgan, S., Lang, S.Q., Schrenk, M.O., Brazelton, W.J., Akizawa, N., Boschi, C., Dunkel, K.G., Quéméneur, M., Whattam, S. A., Mayhew, L., Harris, M., Bayrakci, G., Behrmann, J.H., Herrero-Bervera, E., Hesse, K., Liu, H.Q., Ratnayake, A.S., Twing, K., Weis, D., Zhao, R., Bilenker, L., 2018. Magmatism, serpentinization and life: Insights through drilling the Atlantis Massif (IODP Expedition 357). Lithos 323.

Fujii, T., Moynier, F., Pons, M.-L., Albarède, F., 2011. The origin of Zn isotope fractionation in sulfides. Geochim. Cosmochim. Acta 75, 7632–7643.

Fujii, T., Moynier, F., Abe, M., Nemoto, K., Albarède, F., 2013. Copper isotope fractionation between aqueous compounds relevant to low temperature geochemistry and biology. Geochim. Cosmochim. Acta 110, 29–44.

Fujii, T., Moynier, F., Blichert-Toft, J., Albarède, F., 2014. Density functional theory estimation of isotope fractionation of Fe, Ni, Cu, and Zn among species relevant to geochemical and biological environments. Geochim. Cosmochim. Acta 140, 553–576.

Gaggero, L., Cortesogno, L., Gazzotti, M., 1997. 30. Data reports: Oxides, sulfides, and asociated phases in veins and hydrothermally aletred peridotitic rocks. Proc. ODP Sci. Results 153, 523–529.

Garrido, C.J., Bodinier, J.-L., 1999. Diversity of mafic rocks in the Ronda peridotite: evidence for pervasive melt–rock reaction during heating of subcontinental lithosphere by upwelling asthenosphere. J. Petrol. 40, 729–754.

Godard, M., Lagabrielle, Y., Alard, O., Harvey, J., 2008. Geochemistry of the highly depleted peridotites drilled at ODP Sites 1272 and 1274 (Fifteen-Twenty Fracture Zone, Mid-Atlantic Ridge): Implications for mantle dynamics beneath a slow spreading ridge. Earth Planet. Sci. Lett. 267, 410–425.

Grimes, C.B., John, B.E., Cheadle, M.J., Wooden, J.L., 2008. Protracted construction of gabbroic crust at a slow spreading ridge: Constraints from 206Pb/238U zircon ages from Atlantis Massif and IODP Hole U1309D (30 N, MAR). Geochemistry, Geophysics, Geosystems, p. 9.

Guinoiseau, D., Gélabert, A., Allard, T., Louvat, P., Moreira-Turcq, P., Benedetti, M.F., 2017. Zinc and copper behaviour at the soil-river interface: new insights by Zn and Cu isotopes in the organic-rich Rio Negro basin. Geochim. Cosmochim. Acta 213, 178–197.

Huang, J., Huang, F., Wang, Z., Zhang, X., Yu, H., 2017a. Copper isotope fractionation during partial melting and melt percolation in the upper mantle: Evidence from massif peridotites in Ivrea-Verbano Zone, Italian Alps. Geochim. Cosmochim. Acta 211, 48–63.

Huang, J., Chen, S., Zhang, X.-C., Huang, F., 2018. Effects of Melt Percolation on Zn Isotope Heterogeneity in the Mantle: Constraints From Peridotite Massifs in Ivrea-Verbano Zone, Italian Alps. J. Geophys. Res. Solid Earth 123, 2706–2722.

Huang, J., Ackerman, L., Zhang, X.-C., Huang, F., 2019. Mantle Zn Isotopic Heterogeneity Caused by Melt-Rock Reaction: Evidence From Fe-Rich Peridotites and Pyroxenites From the Bohemian Massif, Central Europe. J. Geophys. Res. Solid Earth 124, 3588–3604.

Huang, R., Song, M., Ding, X., Zhu, S., Zhan, W., Sun, W., 2017b. Influence of pyroxene and spinel on the kinetics of peridotite serpentinization. J. Geophys. Res. Solid Earth 122, 7111–7126 https://doi.org/https://doi.org/10.1002/2017JB014231.

Humphris, S.E., Klein, F., 2018. Progress in Deciphering the Controls on the Geochemistry of Fluids in Seafloor Hydrothermal Systems. Ann. Rev. Mar. Sci. 10, 315–343.

John, S.G., Rouxel, O.J., Craddock, P.R., Engwall, A.M., Boyle, E.A., 2008. Zinc stable isotopes in seafloor hydrothermal vent fluids and chimneys. Earth Planet. Sci. Lett. 269, 17–28.

Karson, J.A., Thompson, G., Humphris, S.E., Edmond, J.M., Bryan, W.B., Brown, J.R., Winters, A.T., Pockalny, R.A., Casey, J.F., Campbell, A.C., 1987. Along-axis variations in seafloor spreading in the MARK area. Nature 328, 681–685.

Kelemen, P.B., Kikawa, E., Miller, D.J., Party, S.S., 2007. Leg 209 summary: Processes in a 20-km-thick conductive boundary layer beneath the Mid-Atlantic Ridge, 14–16 N. In: In: Proceedings of the Ocean Drilling Program, Scientific Results. Ocean Drilling Program College Station, pp. 1–33.

Kempton, P.D., Mathur, R., Harmon, R.S., Bell, A., Hoefs, J., Shaulis, B., 2022. Cu-Isotope Evidence for Subduction Modification of Lithospheric Mantle. Geochemistry, Geophysics, Geosystems, p. 23.

Lissenberg, J., McCaig, A.M., Lang, S.Q., Blum, P., and the IODP Exp 399 Scientific Party, 2024. A long section of serpentinized depleted mantle peridotite. Science.

Liu, S.-A., Huang, J., Liu, J., Wörner, G., Yang, W., Tang, Y.-J., Chen, Y., Tang, L., Zheng, J., Li, S., 2015a. Copper isotopic composition of the silicate Earth. Earth Planet. Sci. Lett. 427, 95–103.

Liu, S.-A., Liu, P.-P., Lv, Y., Wang, Z.-Z., Dai, J.-G., 2019. Cu and Zn isotope fractionation during oceanic alteration: Implications for Oceanic Cu and Zn cycles. Geochim. Cosmochim. Acta 257, 191–205.

Liu, X., Xiong, X., Audétat, A., Li, Y., 2015b. Partitioning of Cu between mafic minerals, Fe–Ti oxides and intermediate to felsic melts. Geochim. Cosmochim. Acta 151, 86–102.

Luguet, A., Alard, O., Lorand, J.P., Pearson, N.J., Ryan, C., O'Reilly, S.Y., 2001. Laser-ablation microprobe (LAM)-ICPMS unravels the highly siderophile element geochemistry of the oceanic mantle. Earth Planet. Sci. Lett. 189, 285–294.

McCoy-West, A.J., Fitton, J.G., Pons, M.-L., Inglis, E.C., Williams, H.M., 2018. The Fe and Zn isotope composition of deep mantle source regions: Insights from Baffin Island picrites. Geochim. Cosmochim. Acta 238, 542–562.

McDonough, W.F., Sun, S., 1995. The composition of the Earth. Chem. Geol. 120, 223–253.

Mével, C., Cannat, M., Gente, P., Marion, E., Auzende, J.M., Karson, J.A., 1991. Emplacement of deep crustal and mantle rocks on the west median valley wall of the MARK area (MAR, 23°N). Tectonophysics 190, 31–53.

Moeller, K., Schoenberg, R., Pedersen, R., Weiss, D., Dong, S., 2012. Calibration of the new certified reference materials ERM-AE633 and ERM-AE647 for copper and IRMM-3702 for zinc isotope amount ratio determinations. Geostand. Geoanal. Res. 36, 177–199.

Moynier, F., Vance, D., Fujii, T., Savage, P., 2017. The isotope geochemistry of zinc and copper. Rev. Mineral. Geochem. 82, 543–600.

Othman, D.B., Luck, J.M., Bodinier, J.L., Arndt, N.T., Albarede, F., 2006. Cu–Zn isotopic variations in the Earth's mantle. Geochim. Cosmochim. Acta 18, A46.
Pak, S.-J., Moon, J.-W., Kim, J., Chandler, M.T., Kim, H.-S., Son, J., Son, S.-K., Choi, S.K., Baker, E.T., 2017. Widespread tectonic extension at the Central Indian Ridge between 8°S and 18°S. Gondw. Res. 45, 163–179.
Palmer, M.R., Edmond, J.M., 1989. Cesium and rubidium in submarine hydrothermal fluids: Evidence for recycling of alkali elements. Earth Planet. Sci. Lett. 95, 8–14.
Patten, C.G.C., Pitcairn, I.K., Teagle, D.A.H., Harris, M., 2016. Sulphide mineral evolution and metal mobility during alteration of the oceanic crust: Insights from ODP Hole 1256D. Geochim. Cosmochim. Acta 193, 132–159.
Paulick, H., Bach, W., Godard, M., De Hoog, J.C.M., Suhr, G., Harvey, J., 2006. Geochemistry of abyssal peridotites (Mid-Atlantic Ridge, 15 20′ N, ODP Leg 209): implications for fluid/rock interaction in slow spreading environments. Chem. Geol. 234, 179–210.
Poitrasson, F., Delpech, G., Grégoire, M., 2013. On the iron isotope heterogeneity of lithospheric mantle xenoliths: implications for mantle metasomatism, the origin of basalts and the iron isotope composition of the Earth. Contrib. Miner. Petrol. 165, 1243–1258.
Pons, M.-L., Quitté, G., Fujii, T., Rosing, M.T., Reynard, B., Moynier, F., Douchet, C., Albarède, F., 2011. Early Archean serpentine mud volcanoes at Isua, Greenland, as a niche for early life. Proc. Natl. Acad. Sci. 108, 17639–17643.
Richter, F.M., Dauphas, N., Teng, F.-Z., 2009. Non-traditional fractionation of non-traditional isotopes: Evaporation, chemical diffusion and Soret diffusion. Chem. Geol. 258, 92–103.
Rouxel, O., Fouquet, Y., Ludden, J.N., 2004. Copper Isotope Systematics of the Lucky Strike, Rainbow, and Logatchev Sea-Floor Hydrothermal Fields on the Mid-Atlantic Ridge. Econ. Geol. 99, 585–600.
Savage, P.S., Moynier, F., Chen, H., Shofner, G., Siebert, J., Badro, J., Puchtel, I.S., 2015. Copper isotope evidence for large-scale sulphide fractionation during Earth's differentiation. Geochem. Perspect. Lett.
Scott, S.R., Sims, K.W.W., Frost, B.R., Kelemen, P.B., Evans, K.A., Swapp, S.M., 2017. On the hydration of olivine in ultramafic rocks: Implications from Fe isotopes in serpentinites. Geochim. Cosmochim. Acta 215, 105–121.
Sossi, P.A., Halverson, G.P., Nebel, O., Eggins, S.M., 2015. Combined separation of Cu, Fe and Zn from rock matrices and improved analytical protocols for stable isotope determination. Geostand. Geoanal. Res. 39, 129–149.
Sossi, P.A., Nebel, O., O'Neill, H.S.C., Moynier, F., 2018. Zinc isotope composition of the Earth and its behaviour during planetary accretion. Chem. Geol. 477, 73–84.
Sossi, P.A., O'Neill, H.S.C., 2017. The effect of bonding environment on iron isotope fractionation between minerals at high temperature. Geochim. Cosmochim. Acta 196, 121–143.
Telus, M., Dauphas, N., Moynier, F., Tissot, F.L.H., Teng, F.-Z., Nabelek, P.I., Craddock, P. R., Groat, L.A., 2012. Iron, zinc, magnesium and uranium isotopic fractionation during continental crust differentiation: The tale from migmatites, granitoids, and pegmatites. Geochim. Cosmochim. Acta 97, 247–265.
Teng, F.-Z., Dauphas, N., Helz, R.T., Gao, S., Huang, S., 2011. Diffusion-driven magnesium and iron isotope fractionation in Hawaiian olivine. Earth Planet. Sci. Lett. 308, 317–324.
Tilhac, R., Ceuleneer, G., Griffin, W.L., O'Reilly, S.Y., Pearson, N.J., Benoit, M., Henry, H., Girardeau, J., Grégoire, M., 2016. Primitive arc magmatism and delamination: petrology and geochemistry of pyroxenites from the Cabo Ortegal Complex, Spain. J. Petrol. 57, 1921–1954.
Tilhac, R., Hidas, K., Oliveira, B., Garrido, C.J., 2023. Evidence of ghost plagioclase signature induced by kinetic fractionation of europium in the Earth's mantle. Nat. Commun. 14, 1099.
Van Dover, C.L., 2019. Inactive sulfide ecosystems in the deep sea: a review. Front. Mar. Sci. 6, 461.
Wang, Z.-Z., Liu, S.-A., Liu, J., Huang, J., Xiao, Y., Chu, Z.-Y., Zhao, X.-M., Tang, L., 2017. Zinc isotope fractionation during mantle melting and constraints on the Zn isotope composition of Earth's upper mantle. Geochim. Cosmochim. Acta 198, 151–167.
Wang, Y., Wu, Z., Huang, Y., Sun, X., Yan, J., Yang, F., Yin, Z., Xu, L., 2023. Fe-Cu-Zn Isotopic Compositions in Polymetallic Sulfides from Hydrothermal Fields in the Ultraslow-Spreading Southwest Indian Ridge and Geological Inferences. Minerals.
Weyer, S., Ionov, D.A., 2007. Partial melting and melt percolation in the mantle: The message from Fe isotopes. Earth Planet. Sci. Lett. 259, 119–133.
Williams, H.M., Bizimis, M., 2014. Iron isotope tracing of mantle heterogeneity within the source regions of oceanic basalts. Earth Planet. Sci. Lett. 404, 396–407.
Workman, R.K., Hart, S.R., 2005. Major and trace element composition of the depleted MORB mantle (DMM). Earth Planet. Sci. Lett. 231, 53–72.
Zhao, X.-M., Zhang, H.-F., Zhu, X.-K., Zhu, B., Cao, H., 2015. Effects of melt percolation on iron isotopic variation in peridotites from Yangyuan, North China Craton. Chem. Geol. 401, 96–110.
Zhao, X., Zhang, Z., Huang, S., Liu, Y., Li, X., Zhang, H., 2017. Coupled extremely light Ca and Fe isotopes in peridotites. Geochim. Cosmochim. Acta 208, 368–380.
Zou, Z., Wang, Z., Li, M., Becker, H., Geng, X., Hu, Z., Lazarov, M., 2019. Copper Isotope variations during magmatic migration in the mantle: insights from mantle pyroxenites in Balmuccia Peridotite Massif. J. Geophys. Res. Solid Earth 124, 11130–11149.
Zou, Z., Wang, Z., Xu, Y.-G., Ciazela, J., Wang, X., Foley, S., Zhang, W.-Q., Li, W., Li, M., Liu, Y., 2024. Contrasting Cu isotopes in mid-ocean ridge basalts and lower oceanic crust: Insights into the oceanic crustal magma plumbing systems. Earth Planet. Sci. Lett. 627, 118563.